Published online 28 September 2021

Nucleic Acids Research, 2021, Vol. 49, No. 19 ***10911–10930***
https://doi.org/10.1093/nar/gkab819

Cockayne syndrome group A and ferrochelatase finely tune ribosomal gene transcription and its response to UV irradiation

Manuela Lanzafame[1,†], Giulia Branca[1,†], Claudia Landi[2], Mingyue Qiang[3], Bruno Vaz[1], Tiziana Nardo[1], Debora Ferri[1], Manuela Mura[1], Sebastian Iben[3], Miria Stefanini[1], Fiorenzo A. Peverali[1], Luca Bini[2] and Donata Orioli[1,*]

[1]Institute of Molecular Genetics -L.L. Cavalli Sforza, CNR, 27100 Pavia, Italy, [2]Department of Life Sciences, University of Siena, 53100 Siena, Italy and [3]Department of Dermatology and Allergic Diseases, Ulm University, Albert-Einstein Allee 23, 89081 Ulm, Germany

Received January 05, 2021; Revised August 10, 2021; Editorial Decision September 03, 2021; Accepted September 12, 2021

ABSTRACT

CSA and CSB proteins are key players in transcription-coupled nucleotide excision repair (TC-NER) pathway that removes UV-induced DNA lesions from the transcribed strands of expressed genes. Additionally, CS proteins play relevant but still elusive roles in other cellular pathways whose alteration may explain neurodegeneration and progeroid features in Cockayne syndrome (CS). Here we identify a CS-containing chromatin-associated protein complex that modulates rRNA transcription. Besides RNA polymerase I (RNAP1) and specific ribosomal proteins (RPs), the complex includes ferrochelatase (FECH), a well-known mitochondrial enzyme whose deficiency causes erythropoietic protoporphyria (EPP). Impairment of either CSA or FECH functionality leads to reduced RNAP1 occupancy on rDNA promoter that is associated to reduced 47S pre-rRNA transcription. In addition, reduced *FECH* expression leads to an abnormal accumulation of 18S rRNA that in primary dermal fibroblasts from CS and EPP patients results in opposed rRNA amounts. After cell irradiation with UV light, CSA triggers the dissociation of the CSA–FECH–CSB–RNAP1–RPs complex from the chromatin while it stabilizes its binding to FECH. Besides disclosing a function for FECH within nucleoli, this study sheds light on the still unknown mechanisms through which CSA modulates rRNA transcription.

GRAPHICAL ABSTRACT

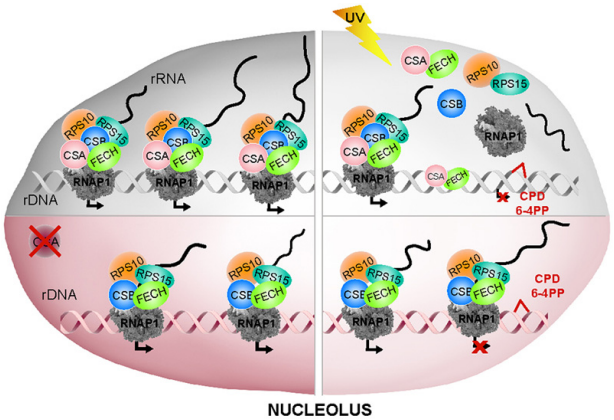

INTRODUCTION

Biallelic mutations in either *ERCC8/CSA* or *ERCC6/CSB* gene are causative of Cockayne syndrome (CS), a segmental progeroid disorder characterized by pre- or post-natal growth failure and progressive neurological degeneration. The disease is clinically heterogeneous with a wide range in type and severity of symptoms that include sensorineural hearing loss, cataracts, dental caries, muscle weakness, decreased subcutaneous adipose tissue, early atherosclerosis, skeletal abnormalities and cutaneous photosensitivity (1–3). The complexity of the pathological clinical presentation in CS is likely linked to the multiple cellular functions of CS proteins, which are not yet fully elucidated. CSA and CSB play a key role in the sub-pathway of nucleotide excision repair (NER), termed transcription cou-

*To whom correspondence should be addressed. Tel: +39 0382 546330; Email: orioli@igm.cnr.it
†The authors wish it to be known that, in their opinion, the first two authors should be regarded as Joint First Authors.
Present addresses:
Bruno Vaz, The European Center for Brain Research, Santa Lucia Foundation, Roma, Italy.
Manuela Mura, Fondazione IRCCS Policlinico San Matteo, Pavia, Italy.

ple repair (TC-NER), that rapidly removes the DNA helix-distorting lesions and the ultraviolet (UV)-induced DNA photoproducts blocking the progression of the transcription machinery in active genes (4). In particular, CSB is an ATP-dependent chromatin-remodelling factor that recruits NER proteins at the site of DNA damage through the interaction with the stalled RNA polymerase II (RNAP2) (5). By binding to DDB1, CUL4A and ROC1 proteins, CSA forms an E3–ubiquitin ligase complex (CSA-core complex) that is required for lesion removal and proteasome-dependent degradation of CSB and subsequent transcription recovery (6–8). Defective TC–NER pathway accounts for the increased cellular sensitivity to the lethal effects of UV light and inability to recover DNA and RNA synthesis at late times after irradiation in CS cells ((9) and references therein). Besides TC-NER, CS proteins are involved in other cellular pathways. It was shown that CSB acts as an auxiliary factor in base excision repair (BER), the major pathway that removes nuclear and mitochondrial oxidative DNA lesions, such as 8-hydroxyguanine (8-OH-Gua) (10–13). It is involved in mitochondrial impairments and cellular senescence *via* regulation of p21 and HTRA3 protease expression (14). Moreover, CSB plays a role in nuclear transcription by interacting with RNAP1 and RNAP2 (15–21) and mediates the transcriptional programs following exposure to cellular stressors such as UV, oxidative damage, inflammation and hypoxia (22). CSB repositions nucleosomes by interacting with NAP1-like histone chaperones (23) and solves the G-quadruplex structures of ribosomal DNA (24). Less detailed information is available on CSA functioning outside TC-NER but, similarly to CS-B, fibroblasts from CSA-defective (CS-A) patients are hypersensitive to oxidative agents, contain high levels of reactive oxygen species (ROS) and are characterized by mitochondrial dysfunction (25–30). Moreover, CSA acts as transcription factor of RNAP1 inside the nucleoli and stimulates RNAP1 transcription re-initiation by recruiting CSB and the TFIIH transcription factor at ribosomal gene promoters 1 (31). Both CSA and CSB favour the RNAP1 recruitment at the rDNA coding region by interacting with the nucleolar protein Nucleolin (32) while the relevance of CS proteins in RNAP1 transcription is highlighted by the recent observations that ribosomal transcription defects are responsible for a loss of proteostasis in CS cells (33–35).

To better understand the molecular mechanisms and the signalling pathways by which CSA operates, we developed a cell system that allowed the identification of a chromatin-bound complex containing RNAP1, CSA, CSB, ribosomal protein (RP) 10, RP15 and ferrochelatase (FECH). FECH is a well-known enzyme (heme-synthase) that catalyses the last step of the heme biosynthesis pathway in mitochondria. Pathogenic mutations in the *FECH* gene cause erythropoietic protoporphyria (EPP, OMIM 177000), an inherited disorder characterized by painful cutaneous photosensitivity as well as severe hepatic disease in 1–5% of patients, which may require treatment by orthotopic liver transplantation (reviewed in (36–39). Besides demonstrating that FECH is a novel interactor of CSA, we find that this heme-synthase protein also localizes in the nucleolus where, in combination with CS proteins, it binds to RNAP1 and regulates ribosomal biogenesis.

MATERIALS AND METHODS

Cell culture conditions and treatments

The study was performed on primary dermal fibroblasts established from biopsies taken from sun-unexposed areas of the skin of CS4PV, CS7PV, CS11PV, CS15PV (CS-A), CS1PV, CS26PV, CS27PV, CS1PL (CS-B) and GM05008 (EPP) patients and from four healthy donors C3PV, C5BO, Fb1609 and Fb377.

In addition, the SV40-transformed MRC5 (normal) and CS3BE.S3.G1 (CS-A) cell lines were used. MRC5 cells were a gift from A. Lehmann (University of Sussex, U.K.) whereas CS3BE.S3.G1 fibroblasts were from the Coriell Cell Repository. CS3BE.S3.G1 cells were used to generate the isogenic cell lines CS3BE-cassette1 and CS3BE-wtCSA$^{Flag\text{-}HA}$. Cells were routinely cultured at 37°C in a humidified atmosphere conditioned with 5% CO_2 and grown in DMEM (Gibco) supplemented with 10% fetal bovine serum (FBS, South America Origin, Gibco), 2 mM L-glutamine (EuroClone), 0.1 mg/ml Streptomycin (EuroClone) and 100 U/ml Penicillin (EuroClone). CS3BE-cassette1 and CS3BE-wtCSA$^{Flag\text{-}HA}$ cell lines were routinely cultured in medium supplemented with 0.25 mg/ml G418 (geneticin, Gibco) or 0.15 μg/ml puromycin (Thermo Fischer Scientific), respectively.

Where indicated, cells were exposed to UV-C light and analysed after recovery in DMEM complete medium for the indicated times. Alternatively, cells were treated with potassium bromate 20 mM (Sigma-Aldrich) or menadione 100 μM (Sigma-Aldrich) in DMEM for 1 h at 37°C.

Cell survival assay

Cell survival was determined by standard clonogenic assays. Briefly, cells were incubated overnight in standard medium supplemented with 10% FBS, then exposed to increasing energy levels of UV-C light (5, 10, 15 or 5, 10, 20, 25, 30 and 35 J/m^2) or increasing menadione concentrations (25, 50, 100 and 200 μM), which was maintained for 1 h and then replaced with fresh standard medium supplemented with 10% FBS. Cells were fixed after 10–15 days and stained with Coomassie. The number of clones was counted and expressed as a percentage of the number of clones in the corresponding untreated cultures.

UDS and RRS

DNA repair capacity in responses to UV irradiation in primary fibroblasts was determined by unscheduled DNA synthesis (UDS) and recovery repair synthesis (RRS) as previously described (40–43).

Plasmids

The pL1Neo-Tk-L2 plasmid (*cassette1*) was generated by cloning the Herpes virus simplex 1 Thymidine kinase (HSV-*tk*) transcription unit from the pTK2A vector (44) into the pEGFP-N1 plasmid (BD Biosciences Clontech, GenBank acc, N, U55762), which contains the selection marker conferring resistance to G418 (*Neo* gene). The DNA fragment

containing the two selection markers was flanked by the heterotypic Cre-recombinase target sites, *loxP* and *lox2272*.

The pRMCE2-wtCSA$^{Flag\text{-}HA}$ plasmid (*cassette2*) was obtained by transferring the *wtCSA$^{Flag\text{-}HA}$* cDNA sequence into the expression vector pRMCE-OriC-ECT-RfA (patent ITMI20120489A1). The *wtCSA$^{Flag\text{-}HA}$* sequence was obtained from the pcDNA3-CSA$^{Flag\text{-}HA}$ (kindly given by K. Tanaka, Osaka University, Japan), cloned into the Gateway entry vector pENTR™11 (Thermo Fischer Scientific) and then transferred to the pRMCE-OriC-ECT-RfA vector by LR recombination reaction (Gateway system, Thermo Fischer Scientific) following manufacturer instructions. Recombination reaction was set up with 65 ng pENTR11-CSA$^{Flag\text{-}HA}$, 150 ng pRMCE–OriC–ECT–RfA, 2 μl 5× LR Clonase reaction buffer in TE buffer (10 mM Tris–Cl pH 7.5, 1 mM EDTA).

The pRMCE–OriC–ECT–RfA plasmid derives from the *pBKS-eLamB2-ori*, which carries the ectopic 1.2 kb *LaminB2* origin of DNA replication (here indicated as *ECT* sequence) (45). The SV40-driven *pac* transcription unit isolated from the pPur vector (BD Biosciences Clontech) and the CMV-driven *RfA* transcription unit (Thermo Fischer Scientific) were cloned in opposite direction at each side of the *ECT* sequence. The DNA fragment containing the *pac*, *ECT* and *RfA* sequences were flanked by *loxP* and *lox2272* sites.

The pCre express the NLS-Cre recombinase under the HSV-*tk* promoter. It was isolated from the pCre/Flp, gifted by Dr Lauth M (46), by digestion with HindIII and SalI, and cloned into pBluescript KS (+) (Stratagene).

Generation of the CS3BE-derivative cell lines

The CS3BE-cassette1 cell line was obtained by transfecting CS3BE.S3.G1 cells with 2.5 μg of the BamH1-linearized pL1Neo-Tk-L2 plasmid (*cassette1*) by using the Lipofectamine LTX and Plus reagent (Thermo Fischer Scientific), according to manufacturer instructions. After G418 selection, resistant clones were isolated and PCR-screened for the presence of both *loxP* and *lox2272* recombination sites.

Single copy integration of *cassette1* was verified by Southern blot analysis. Briefly, genomic DNA was purified by phenol:chloroform:isoamyl alcohol (25:24:1) extraction in Eppendorf Phase-Lock Gel™ Light and sodium acetate (1/10 volume)/ethanol 100% (2.5 volume) precipitation. About 12 mg of DNA were then digested with 72 IU EcoRI or BglII restriction enzymes, fractionated on 0.8% TBE-agarose electrophoresis, blotted onto a Hybond N^+ membrane (Amersham Pharmacia) and probed with ^{32}P-labelled PvuI-linearized *pTk2A*. Filters were exposed to phosphoimager cassettes and the autoradiographic signal was acquired by Typhoon Trio scanner (GE Healthcare).

CS3BE-cassette1 clone 68 cells were used to generate the CS3BE-wtCSA$^{Flag\text{-}HA}$ cell line by *Recombinase-Mediated Cassette Exchange*. Briefly, CS3BE-cassette1 cells at 90–95% of confluence were co-transfected with 2 μg pCre and 2 μg pRMCE2-wtCSA$^{Flag\text{-}HA}$ (*cassette2*) by using the Lipofectamine™ LTX and Plus™ reagent (Thermo Fischer Scientific) according to manufacturer instructions. Forty-eight hours later, recombined cells were selected in 0.3 μg/ml puromycin containing medium and two days later, GCV (2 μg/ml) was added to the medium in order to counter-select against random integration of *cassette2*. Parallel aliquots of positive clones were also checked for G418 sensitivity.

Polymerase chain reaction (PCR)

To identify clones that stably integrated a single-copy of *cassette1* (CS3BE-cassette1) or that successfully recombined *cassette2* (CS3BE-wtCSA$^{Flag\text{-}HA}$) by Cre-mediated RMCE, PCR-screening was carried out on genomic DNA isolated from single colonies by lysing cells in H_2O, freezing and thawing them in dry ice and at 95°C for 10 min, respectively. After proteinase K treatment, PCR reactions were carried out in 50 μl containing 1× GoTaq Master Mix Reaction mix (Promega), 2.5 mM each dNTPs, 20 pmol each primer, either 1 or 3 mM $MgCl_2$ (see Supplementary Table S1) and 1 U GoTaq DNA polymerase (Promega). Amplification was performed with one cycle of initial denaturation at 94°C for 3 min, forty cycles at 94°C for 30 s, annealing temperature for 30 s and 72°C for 30 s, and a final extension at 72°C for 5 min. Primer sequences are listed in Supplementary Table S1.

RNA extraction and real time RT–PCR analysis

Analyses were performed according to standard protocols (47). Total RNA was extracted from cells using the RNeasy kit (Qiagen) according to the manufacturer's instructions. Contaminant DNA was removed by treatment with DNase I (Qiagen), and in a single RT reaction, 1 μg RNA was reverse transcribed using the iScript cDNA synthesis kit (BioRad). The cDNAs were used as template in real-time PCR reactions containing 10 pmol each forward and reverse primers (Supplementary Table S2) and the SYBR Green I fluorescent dye (Biorad). The PCR reactions were performed in the LightCycler 480 Real-Time PCR system (Roche Diagnostics).

Cloning of the genomic integration site (SpacerC3-PCR assay)

High resolution mapping of the genomic integration site of the transgenic vector was obtained by applying a modified-splinkerette assay (48). Briefly, the splinkerette Top oligonucleotide was replaced by the SPL-TOP-GATC-5′P-spC3 (5′[PHO] GATCCCACTAGTGTCGACACCAGTCTC [SpC3] 3′) oligonucleotide and annealed with the SPLNK-BOT2 (5′-CGAAGAGTAACCGTTGCTAGGAGAGACCGTGG CTGAATGAGACTGGTGTCGACACTAGTGG-3′) oligonucleotide. Annealed double strand linker, spC3-GATC-linker, was obtained by mixing the above (40μM/each) oligonucleotides in the annealing buffer (10 mM Tris pH 7.5, 50 mM NaCl, 10 mM $MgCl_2$), heating at 95°C for 2 min and slowly cooling at room temperature. The linker was then diluted in water to the 4 μM final stock concentration. In parallel, CS3BE-wtCSAFlag-HA genomic DNA (gDNA) was purified with standard procedure based on sodium dodecyl-sulphate lysis supplemented with proteinase K followed by rounds of phenol-chloroform extractions. 200 ng of CS3BE-wtCSAFlag-HA gDNA was

digested by BglII (10 U/μg) and ligated to a (0.5 μM) molar excess spC3-GATC-linker with 3 μl T4 DNA Ligase (400 U/ul) NEB in a 50 μl final volume. Ligation was precipitated in 0.3 M sodium acetate pH 5.2 and 3 volume of 95% ethanol. The pellet was resuspended in 10 μl 0.1× TE, and 0.5μl used as template in the first reaction of the three serial PCR (nested-PCR) with FDM-003-fw/ SPLNK#1_S1 (PCR525) primer set. The second and third serial PCRs were then performed with FDM-005_fw/ SPLNK#1_S2 (PCR534) and FDM-006_fw/ SPLNK#1_S2 (PCR535) primer sets on 1:20 dilutions of the PCR525 and PCR534 templates, respectively. Primer sequences are listed in Supplementary Table S3.

The plasmid-genomic-linker chimeric PCR product was then sequenced by standard procedure. To confirm the cloning of the integration site and exclude artefactual chimeric DNA generated by the ligation step, PCR reactions performed with primer sets targeting the 5′ (Supplementary Table S4) or 3′ (Supplementary Table S5) arms of the vector or the flanking gDNA sequences (Supplementary Table S6) were assayed on undigested gDNA.

RNA interference

Primary fibroblasts were transfected with 75mM control (AllStars Negative Control siRNA, 1027280, Qiagen), *FECH* siRNA (Hs_FECH_1 SI00002898, Hs_FECH_2 SI00002905, Hs_FECH_3 SI00002912, Hs_FECH_5 SI03023090 FlexiTube siRNA, Qiagen), *ERCC8/CSA* siRNA (Hs_ERCC8_9 SI03089492, Hs_ERCC8_8 SI03051713, Hs_ERCC8_7 SI03025456, Hs_ERCC8_3 SI00001617 FlexiTube siRNA, Qiagen), *RPS10* siRNA (Hs_RPS10_8 SI04270196, Hs_RPS10_7 SI04193588, Hs_RPS10_5 SI02731071, Hs_RPS10_2 SI00707126 FlexiTube siRNA, Qiagen) or *RPS15* siRNA (Hs_RPS15_10 SI04326140, Hs_RPS10_9 SI04183256, Hs_RPS10_8 SI03208730, Hs_RPS10_3 SI00707273 FlexiTube siRNA, Qiagen) using the HiPerFect Transfection Reagent (301705, Qiagen). After 60 h, a second transfection was performed with the same siRNA and procedure. Cells were processed after 120 h of gene silencing.

Immunofluorescence

Cells were fixed with 3.7% paraformaldehyde (PFA) for 12 min, permeabilized in PBS containing 0.1% Triton X-100, hybridized with anti-HA (Roche, 11867423001; 1:250), anti-FECH (S. Cruz, sc-377377; 1:40) or anti-TOMM 20 (Sigma) antibodies and afterwards with secondary antibodies conjugated to Alexa Fluor 448 or Alexa Fluor 555 (Jackson Immunoresearch). Nuclei were counterstained with DAPI. Images were acquired using an Olympus IX71 inverted microscope equipped with a CCD camera (Robert Scientific Photometrics) and analysed using the MetaMorph Microscopy Automation and Image Analysis Software (Molecular Devices). The quantification of FECH accumulation inside the nucleolus was performed on immunostained cells 1, 2, 3 or 4 h after UV-C irradiation (10 J/m^2). For each cell strain, at least 200 nuclei were analysed. Exposure time, binning, microscope settings and light-source intensity were kept constant for all the samples.

Proximity ligation assay (PLA)

CS3BE-cassette1 or CS3BE-wtCSA$^{Flag\text{-}HA}$ cells were fixed with 3% PFA for 12 min at RT and subsequently permeabilized with 0.1% Triton X-100 in PBS at the indicated time points after UV-C irradiation (10 J/m^2). PLA was performed by using the Duolink *in situ* Detection Kit (Sigma-Aldrich) following manufacturer's instructions. Briefly, cells were incubated with provided blocking buffer for 30 min at RT, then incubated with anti-HA antibody (Cell Signaling, 3724; 1:1000) and anti-FECH antibodies (S. Cruz, sc-377377; 1:40) or anti-RNAP1 (RPA194, S. Cruz, sc-48385; 1:50) and anti-FECH (Abcam, ab55965; 1:50) and subsequently with anti-mouse PLUS and anti-rabbit MINUS PLA probes. Interaction foci were imaged using an Olympus IX71 inverted microscope equipped with a CCD camera (Robert Scientific Photometrics) and analyzed using the ImageJ software (49).

Run-on transcription assay

BrUTP incorporation in permeabilized cells (Run-on Transcription) was performed as previously described (50). Briefly, cells were seeded on coverslips, washed once with TBS and once with glycerol buffer (20 mM Tris–HCl, pH 7.4, 5 mM $MgCl_2$, 25% glycerol, 0.5 mM PMSF, 0.5 mM EGTA). Cells were then permeabilized with glycerol buffer containing 0.05% Triton X-100 for 3 min at RT and incubated with transcription buffer (100 mM KC1, 50 mM Tris–HCl, pH 7.4, 5 mM $MgC1_2$, 0.5 mM EGTA, 25% glycerol, 5 U/ml RNase inhibitor from human placenta (Boehringer), 1 mM PMSF, 0.5 mM ATP, 0.5 mM of ATP, CTP, GTP (GE Healthcare) and 0.2 mM BrUTP (Sigma-Aldrich)) at RT for 1 h. Samples in which RNAP2 was inhibited were incubated with 200 μM DRB (Sigma-Aldrich) for 1 h at RT, concurrently with transcription reaction. Coverslips were then washed once for 3 min with TBS containing 0.5% Triton X-100 and 5 U/ml RNase inhibitor, and once with TBS containing 5 U/ml RNase inhibitor. Afterwards, cells were fixed in 2% PFA for 15 min and hybridized with fluorescent anti-BrdU antibodies (GeneTex, GTX128091; 1:100). The intensity profiles were achieved by using the MetaMorph Microscopy Automation and Image Analysis Software (Molecular Devices). Nuclei were segmented based on DAPI staining and the signal-integrated density of BrdU staining was quantified for each nucleolar region using ImageJ software (49).

Whole cell extract and subcellular fractionations

Adherent cells were lysed 15 min at RT in Cell Lytic M buffer (Sigma-Aldrich) supplemented with protease inhibitor cocktail (Roche). Whole cell lysate was collected with a cell scraper, centrifuged at 13 000 rpm for 15 min and stored at −20°C.

Nuclear (Nuc) and Cytoplasmic (Cyt) fractions were prepared by using the Nuclear complex Co-IP kit (Active Motif) according to manufacturer's instructions. Briefly, cells were collected by scraping in ice-cold PBS supplemented with phosphate inhibitors (Active Motif), centrifuged, resuspended in hypotonic buffer, incubated for 15 min on ice

and homogenized by 30 strokes with a dounce homogenizer. The homogenate was diluted with detergent buffer and centrifuged at 12 000 rpm for 30 s to recover the supernatant that included both cytosolic and mitochondrial fractions. The nuclear pellet was resuspended in Complete Digestion Buffer (Digestion Buffer supplemented with protease inhibitor cocktail and 0.5 mM PMSF), supplemented with the Enzymatic Shearing Cocktail and incubated at 4°C for 3 h. The reaction was stopped by adding 0.5M EDTA for 5 min on ice. Finally, the suspension was centrifuged at 12 000 rpm for 30 s to recover the supernatant containing the nuclear fraction.

Pure mitochondrial fractions (Mit) were obtained using the Mitochondrial fractionation kit (Active Motif) or the Mitochondria Isolation Kit (Sigma-Aldrich) according to the manufacturer's instructions. Pure nuclear/cytoplasmic fractions (Nuc/Cyt) free from mitochondria were obtained as described in reference (51), steps 13–23.

For nucleolar fractionation, previously described protocols have been adapted in order to guarantee the absence of mitochondrial contamination (51,52). Briefly, 4×10^7 primary dermal fibroblasts from healthy donors were washed in cold PBS, centrifuged and resuspended in five volumes of extraction buffer A (20 mM Tris pH 7.6, 0.1 mM EDTA, 2 mM $MgCl_2$, 0.5 mM NaF and 0.5 mM Na_3VO_4) supplemented with Proteinase Inhibitor Cocktail (PIC). Cell pellet was incubated 10 mins on ice, added 10% (vol/vol) solution of Nonidet P-40 and mixed by tube inversion. Cell membranes were fragmented by passing the lysate through a G-20 needle and intact nuclei were collected by centrifugation at 500g for 3 min at 4°C. Supernatant (cytoplasm) was stored at −80°C. The pellet containing nuclei was resuspended in 2 ml of S1 buffer (0.25 M sucrose, 10 mM $MgCl_2$), layered over 2 ml of S2 buffer (0.35 M sucrose, 0.5 mM $MgCl_2$) and centrifuged at 1430g for 5 min at 4°C. Pellet was again resuspended in 2 ml of S2 buffer and sonicated (6 times alternating 10 s bursts and 10 s rest). After checking the breakup of nuclei with a phase contrast microscope, the sample was layered over 2 ml of S3 buffer (0.88 M sucrose, 0.5 mM $MgCl_2$) and centrifuged at 3000g. The nucleolar pellet was collected while the supernatant (nucleoplasm) was added to the cytoplasm fraction. Nucleoli were resuspended in 1 ml of S2 buffer, centrifuged at 1430g for 5 min at 4°C and finally resuspended in 50 μl of RIPA buffer supplemented with PIC. Nucleolar extract was used for immunoblotting.

Chromatin-enriched fractions were prepared as previously described (53). Cells were lysed in Triton Lysis Buffer (10 mM Tris–HCl pH 7.4, 1% Triton X-100, 2.5 mM $MgCl_2$, 0.025 mM Na_3VO_4, 12.5 mM NaF, 6.25 mM β-glycerophosphate, protease and phosphatase inhibitors) and centrifuged (13 400 rpm) for 5 min at 4°C. The supernatant was collected (soluble fraction) whereas the pellet (chromatin-enriched fraction) was dissolved in WCE buffer (25 mM HEPES pH 7.9, 130 mM NaCl, 1.5 mM MgCl, 0.2 mM EDTA, 0.1% TritonX-100, 0.5 mM DTT, protease and phosphatase inhibitors) and used for immunoblotting.

Immunoblot analysis and silver staining

Whole cell extracts or cellular fractions were supplemented with NuPage LDS sample buffer 1× and 50mM DTT, incubated at 70°C for 10 min and analyzed by SDS-PAGE. For gel electrophoresis the 4–12% NuPAGE Bis-Tris Gels (Thermo Fischer Scientific), 4–20% Mini-Protean TGX Gels (Bio-Rad) or 12% SDS-polyacrilamide gels were used. Samples were transferred onto a nitrocellulose membrane by using the Trans-Blot Turbo transfer system (Bio-Rad). Immunoblotting was performed using antibodies specific for CSA (Genetex, GTX100145; 1:500), CSB (S. Cruz, sc-10459; 1:300), Cul4A (Genetex, GTX113876; 1:500), c-Jun (S. Cruz, sc-1694; 1:500), DDB1 (a gift from Dr R. Groisman; 1:1000), FECH (S. Cruz, sc-377377; 1:250), GAPDH (S. Cruz, sc-32233; 1:1000), HA (Roche, 11867423001; 1:1000), HA (Cell Signaling, 3724; 1:1000), H3 (Abcam, ab1791; 1:10 000), MEK2 (BD Biosciences, 610235; 1:2000), ORC2 (S. Cruz, sc-32734; 1:2000), PCNA (S. Cruz, sc-10807; 1:1000), RNAP1 (S. Cruz, sc-48385; 1:500), ROC1 (Abcam, ab133565; 1:1000), RPSA (Abcam, ab133645; 1:1000), RPS10 (Genetex, GTX33475; 1:1000), RPS15 (Abcam, ab157193; 1:1000), RPS28 (Abcam, ab133963; 1:500), SDHA (Abcam, ab14715; 1:10 000). Chemiluminescent signals were detected using the Chemi-Doc XRS system (Bio-Rad) and quantified using the ImageJ software (49).

For gel silver staining, proteins were resolved on a 4–12% NuPAGE Bis–Tris Mini gel (Thermo Fischer Scientific) and stained with the SilverQuest Silver Staining kit (Thermo Fischer Scientific) following manufacturer instructions.

Single and two-step co-immunoprecipitations

Whole cell lysates or subcellular fractions from $0.3–1 \times 10^7$ cells, were immunoprecipitated with anti-FECH (S. Cruz, sc-377377ac), anti-RNAP1 (S. Cruz, sc-48385ac) or anti-CSB (A301-345A Bethyl) antibodies conjugated with A/G agarose beads according to standard protocols (54). Briefly, extracts were incubated overnight at 4°C with 15 μg of antibody-conjugated beads. Beads were washed three times with 1X IP high buffer (Active Motif) supplemented with 1 mg/ml BSA and three times with 1× IP high buffer. Immunoprecipitated proteins were eluted for 10 min at 70°C with NuPAGE-LDS Sample Buffer 2× (Thermo Fischer Scientific), supplemented with 50 mM DTT and further investigated by immunoblotting.

For the two-step co-immunoprecipitation (TIP), chromatin enriched fractions were first immunoprecipitated with anti-FECH antibody (S. Cruz, sc-377377ac) following the conditions described above. The immunoprecipitated proteins were eluted three times at RT with Ferrochelatase (A-3) blocking peptide (S.Cruz, sc-377377 P) and subsequently immunoprecipitated with anti-RPA194 antibody (S. Cruz, sc-48385ac). Final elution was performed for 10 min at 70°C with NuPAGE-LDS Sample Buffer 2× (Thermo Fischer Scientific) supplemented with 50 mM DTT.

Chromatin-immunoprecipitation

ChIP experiments were performed as described (55). Briefly, DNA co-immunoprecipitated with the anti-RNAP1 antibodies (RPA194, S. Cruz, sc-48385) was quantified by real

time PCR using the primers listed in Supplementary Table S7 and the LightCycler 480 (Roche).

Tandem affinity purification (TAP)

Total extracts from 5×10^7 cells were incubated overnight at 4°C with anti-Flag M2 Affinity Gel (Sigma-Aldrich). Beads were washed five times with 1× IP low buffer (Active Motif) and the immunoprecipitated proteins were eluted with the Flag peptide (Sigma-Aldrich) in TBS (Tris 10 mM pH 7.4, NaCl 150 mM). Eluates were further immunoprecipitated with anti-HA agarose affinity resin (Sigma-Aldrich) overnight at 4°C. Beads were washed 5 times with 1× IP low buffer and the immunoprecipitated proteins were eluted by incubating the beads for 10 min at RT with 2× NuPAGE-LDS Sample Buffer (Thermo Fischer Scientific). Eluates were supplemented with 50 mM DTT and further investigated by immunoblotting.

Mass spectrometry

Total cell extracts from 1×10^9 of CS3BE-cassette1 or CS3BE-wtCSA$^{Flag\text{-}HA}$ cells were subjected to TAP, as described. All samples were loaded and resolved on 9–16% home-made polyacrylamide linear gradient gels (18 × 20 cm × 1.5 mm) at 40 mA/gel constant current, at 9°C (56). Gels were stained according to a MS-compatible silver staining protocol (57) and digitized with Image Scanner III laser densitometer controlled by LabScan 6.0 software (GE Healthcare). Each visible band was manually excised, destained in 2.5 mM ammonium bicarbonate and 50% (v/v) acetonitrile, and 100% (v/v) acetonitrile dehydrated. Before protein digestion, protein bands were reduced with 10 mM DTE in 25 mM ammonium bicarbonate (1 h at 56°C) and then alkylated with 55 mM iodoacetamide in 25 mM ammonium bicarbonate at room temperature (45 min, in darkness). After 10 min of incubation with 50 mM ammonium bicarbonate, protein bands were dehydrated with 100% (v/v) acetonitrile. Dehydrated protein bands were, then, rehydrated in trypsin solution (Sigma Aldrich) and in-gel protein digestion was performed by an overnight incubation at 37°C.

Protein identification was carried out by Peptide Mass Fingerprinting (PMF) on an ultrafleXtreme™ MALDI-ToF/ToF instrument (Brucker Corporation). 1.25 μl of each digested protein solution, from each excised band, was spotted onto the MALDI target and allowed to dry. Then 0.75 μl of matrix solution (5mg/ml alpha-ciano 4 hydroxycynnamic acid in 50% (v/v) acetonitrile and 0.5% (v/v) trifluoroacetic acid) was applied to the dried sample, which was dried again. After acquiring the mass of the peptides, a mass fingerprinting search was carried out in Swiss-Prot/TrEMBL and NCBInr databases using MASCOT search engine available on-line (Matrix Science Ltd). Taxonomy was limited to Homo sapiens, mass tolerance was 50 ppm, and the acceptable number of missed cleavage sites was set at one. Alkylation of cysteine by carbamidomethylation was assumed as a fixed modification and oxidation of methionine was considered as a possible modification. The criteria used to accept identifications included the extent of sequence coverage (>15%), the number of matched peptides (>4) and the MASCOT algorithm assigned probabilistic score (>80 or $P < 0.001$).

Northern blot

Norther blot was performed according to previously described protocols (35,58). Briefly, 5 μg of total RNA was denatured at 65°C for 15 min, placed on ice for 5 min and run on a 0.9% agarose gel for 3 h at 80 V. RNAs were then transferred to Amersham Hybond membrane overnight, crosslinked with 1200 J UV and pre-hybridized for 2 h at 65°C with pre-hybridization buffer (50% formamide, 0.1% SDS, 8× Denhardt's solution, 5× SSC buffer, 50 mM NaP buffer, 0.5 mg/ml t-RNA). The ^{32}P-labeled oligonucleotide probe was denatured at 95°C for 10 min and added to the membrane. After 1 h at 65°C, the membrane was incubated at 37°C overnight, washed in 2× SSC and exposed to an X-ray film. Bands were quantified using ImageQuant Software.

Statistics

All the experiments were repeated at least two-three times. *P*-values were obtained by the unpaired two-tailed student *t*-test. Fisher *F*-ratio at a probability level (*P*-value) of 0.05 was used to compare variances among the analysed groups. Data are reported as mean ± standard error of the mean (SEM). *P*-values <0.05 were considered significantly different.

Bioinformatics nuclear predictions tool

cNLS Mapper tool (59) was used to predict the presence of nuclear localization signal (NLS) specific to the importin αβ pathway in the FECH sequence. NLS scores provided indicate the NLS activities. The NucPred analysis tool (60) was also used to analyse FECH protein sequence and predict whether the protein spends at least some time in the nucleus.

RESULTS

Generation of wtCSA$^{Flag\text{-}HA}$ expressing cells by RMCE

To identify novel CSA interactors, we generated two isogenic cell lines by applying the recombinase mediated cassette exchange (RMCE) technique to the CS3BE cell line (CS-A), which is compound heterozygous for mutations leading to premature stop codons in CSA (p. E13* and p. T134Lfs*13). The isogenic cell lines diverge for the expression of the wild type CSA protein tagged at the C-terminal with Flag and HA epitope tags (wtCSA$^{Flag\text{-}HA}$). At first, we randomly integrated in the genome of the CS3BE cells a single copy of a recipient DNA cassette (*cassette1*) flanked by the heterotypic *lox2272* and *loxP* sites targets of the Cre recombinase (Figure 1). CS3BE clones carrying *cassette1* were positively selected in G418 containing media and screened by PCR and Southern blotting for the presence of a single integration event (Supplementary Figure S1). CS3BE clone 68 (thereby termed CS3BE-cassette1) was then co-transfected with the Cre-expression vector and a DNA plasmid containing the *wtCSA$^{Flag\text{-}HA}$* cDNA flanked

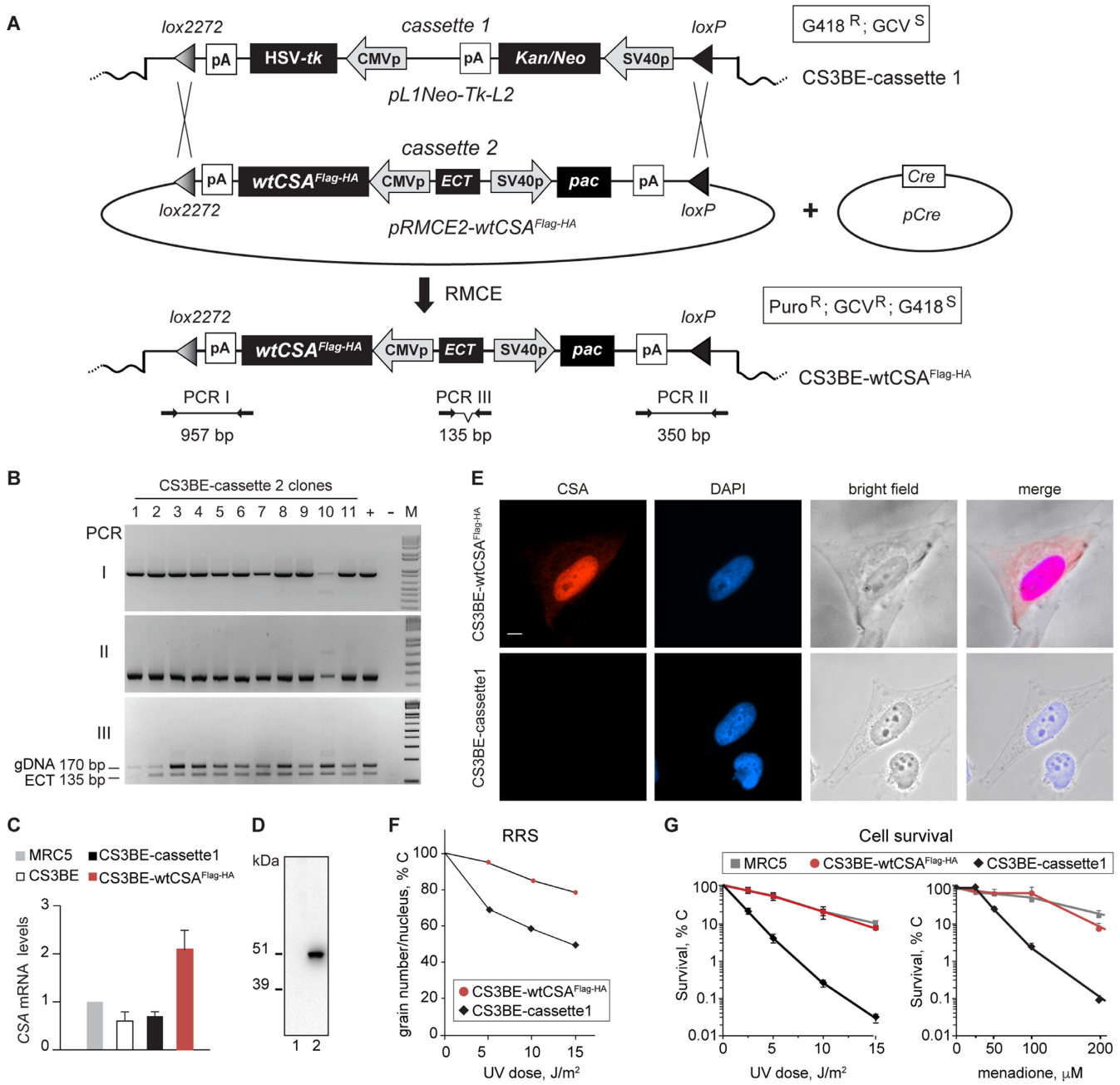

Figure 1. Generation of the CS3BE-wtCSA$^{Flag\text{-}HA}$ cells. (**A**) A single copy of a recipient DNA cassette (*cassette1*) flanked by the heterotypic *loxP*/*lox2272* Cre target sites and carrying positive (Kan/Neo) and negative (HSV-*tk*) selectable markers was randomly integrated in the genome of the CS-A cell line *CS3BE* (CS3BE-cassette1). Co-transfection of CS3BE-cassette1 cells with the plasmids *pRMCE-Ori-ECT-wtCSA* (containing *cassette2*) and *pCre* (expressing the Cre recombinase), allowed the Recombinase-Mediated Exchange of *cassette1* with *cassette2* (RMCE). *Cassette2* contains the wtCSA$^{Flag\text{-}HA}$ cDNA, a positive selectable marker (*pac*) and the *ECT* DNA sequence for stable expression of the flanking genes. Positions of the primers for PCR screening and size of the corresponding products are indicated. *ECT*: ectopic sequence; G418^R: resistance to G418; HSV-*tk*: Herpes simplex Virus 1 thymidine kinase; *Kan*: kanamycin; *Neo*: neomycin; p: promoter; pA: polyadenylation site; Puro^R: puromycin resistance. (**B**) PCR amplifications of amplicon I (*loxP*) and III (*lox2272*) verify the correct RMCE event whereas amplicon II (*ECT* region) distinguishes the single integration event of *cassette2*. *ECT* corresponds to a deleted form of an endogenous LaminB2 origin of replication (45) present on both homologous chromosomes. In case of a single integration of *cassette2*, the PCR assay amplifies the endogenous (170 bp) and the deleted sequence (135 bp) in a 2:1 ratio, as observed in clones number 3, 4, 8 and 10. Positive (+) and negative (−) controls of the PCR reactions are shown. M: DNA ladder. (**C**) *CSA* expression levels in MRC5 (normal), CS3BE (CS-A) and CS3BE-derivative cell lines. Transcript levels were first normalized to *GAPDH* expression levels and afterwards to the values in MRC5 cells. Reported values represent the mean ± SEM. (**D**) Immunoblot analysis with anti-HA antibodies of whole cell extracts from the CS3BE-cassette1 (1) and CS3BE-wtCSA$^{Flag\text{-}HA}$ (2) cells. (**E**) Immunofluorescence analysis with anti-HA antibodies in CS3BE-wtCSA$^{Flag\text{-}HA}$ and CS3BE-cassette1 cells. Nuclei were counterstained with DAPI and cells visualized in bright field. (**F**) Recovery of RNA synthesis (RRS) in CS3BE-wtCSA$^{Flag\text{-}HA}$ and CS3BE-cassette1 cells. The mean numbers of autoradiographic grains per nucleus in irradiated samples are expressed as percentages of those in unirradiated cells. (**G**) Sensitivity to UV-C irradiation or menadione treatment of MRC5 and CS3BE-derivative cell lines. Values in irradiated/treated samples are expressed as percentages of those in unirradiated/control cells. Reported values represent the mean ± SEM ($n = 3$). Scale bar: 5 μm.

by the *loxP* and *lox2272* sites (*cassette2*) (Figure 1A). The Cre recombinase mediated the swapping of *cassette1* with *cassette2* by a site-specific recombination event between the two identical *loxP* sites. Cells containing *cassette2* were selected for their resistance to puromycin ($Puro^R$) and ganciclovir (GCV^R) and for their sensitivity to G418. The recombination process and the single-integration event of *cassette2* in chr9q21.11 were carefully characterized by PCR analysis (Figure 1B) whereas the integration breakpoint was mapped at the nucleotide level (Homo Sapiens chr9: 68 385 454–68 385 486 GRCh38.p12) by a modified version of the splinkerette assay (Supplementary Figure S2). One of the clones showing the proper single copy integration of *cassette2* (clone 4 thereby termed CS3BE-wtCSA$^{Flag\text{-}HA}$) was further investigated for the expression level of *CSA* mRNA. By using primer pairs specific for the *CSA* coding sequence, we evaluated the total amount of *CSA* transcript in CS3BE-wtCSA$^{Flag\text{-}HA}$, CS3BE-cassette1, CS3BE cells and the normal human fibroblasts MRC5 (Figure 1C). The amount of *CSA* transcripts in CS3BE-cassette1 is comparable to that of the parental cell line CS3BE, indicating that the integration of *cassette1* in the genome of CS3BE cells does not alter the expression of the mutated endogenous alleles. In CS3BE-wtCSA$^{Flag\text{-}HA}$ cells, the amount of *CSA* mRNA is twice that of MRC5 cells, indicating similar expression levels for the recombinant wtCSA$^{Flag\text{-}HA}$ and the endogenous *CSA* gene. In addition, anti-HA antibodies recognize a single band of ∼48 kDa corresponding to the molecular weight of the wtCSA$^{Flag\text{-}HA}$ protein (Figure 1D). By immunofluorescence, we found that the recombinant wtCSA$^{Flag\text{-}HA}$ protein is localized mainly in the nucleus with a weaker but still detectable signal in the nucleolus (Figure 1E), as previously reported for the endogenous CSA (18,31).

The functionality of wtCSA$^{Flag\text{-}HA}$ in TC-NER was demonstrated by the higher Recovery of UV-inhibited RNA synthesis (RRS) in CS3BE-wtCSA$^{Flag\text{-}HA}$ cells compared to CS3BE-cassette1 (Figure 1F) and by the higher level of cell viability after UV irradiation or oxidative stress (Figure 1G). While a drastically reduced survival was found in CS3BE-cassette1 cells, an overlapping survival curve was observed between CS3BE-wtCSA$^{Flag\text{-}HA}$ and the control MRC5 cells, indicative that wtCSA$^{Flag\text{-}HA}$ expression fully recovers the hypersensitivity of CS3BE-cassette1 cells to UV as well as oxidative stress.

CSA interacts with the ferrochelatase (FECH) protein inside the nucleus

The sequential use of anti-Flag and anti-HA antibodies allowed the purification of CSA-interacting proteins by Tandem Affinity Purification (TAP) while the identity of the CSA-binding proteins was determined by mass spectrometry. Besides the well-known interactors of CSA implicated in TC-NER (namely, DDB1, Cul4A, CSN1, CSN2, CSN3, CSN4, CSN5, CSN6, CSN7A and 7B, CSN8, Roc1), we isolated several other proteins among which the mitochondrial inner membrane protein ferrochelatase (FECH) (Figure 2A and Supplementary Table S8). Notably, none of the CSA-interacting proteins was found in the parental cell line CS3BE-cassette1. FECH is the terminal enzyme in the heme biosynthesis pathway where it catalyses the insertion of the Fe^{2+} iron into protoporphyrin IX (61,62). Mutations in the *FECH* gene are associated with erythropoietic protoporphyria (EPP), an inherited disease of porphyrin-biosynthesis, characterized by severely painful phototoxic reactions due to the accumulation of protoporphyrin in the blood. Further investigations by TAP assay showed that wtCSA$^{Flag\text{-}HA}$ interacts with FECH as well as with its well-known partner DDB1 (Figure 2B). Accordingly, by using anti-FECH antibodies we found that wtCSA$^{Flag\text{-}HA}$ co-immunoprecipitates with the endogenous FECH whereas no interaction was observed in CS3BE-cassette1 cells (Figure 2C), as expected. Remarkably, in primary dermal fibroblasts from healthy donors, we repeatedly found that not only the endogenous CSA protein but also a barely detectable amount of CSB co-immunoprecipitates with FECH (Figure 2D). Conversely, we were unable to provide reliable evidence of interaction between FECH and components of CSA-core complex, such as DDB1, Cul4A and Roc1, suggesting additional functions of CSA outside the CSA-core complex.

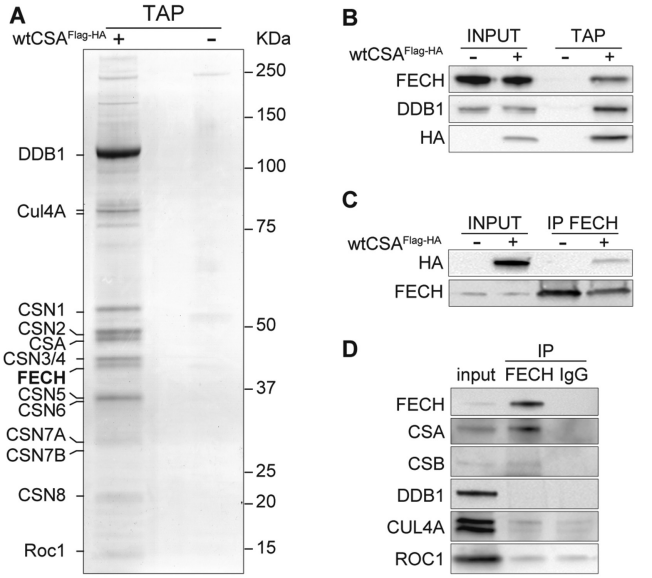

Figure 2. FECH is a novel interactor of CSA. (**A**) Silver staining analysis of CSA-interacting proteins purified from total cell extracts of CS3BE-cassette1 (−) or CS3BE-wtCSA$^{Flag\text{-}HA}$ cells (+) by Tandem Affinity Purification (TAP). The identity of CSA-interacting proteins was determined by mass spectrometry. (**B**) Immunoblot analysis with antibodies specific for FECH, DDB1 or HA of the CSA$^{Flag\text{-}HA}$-interacting proteins isolated by TAP experiments in CS3BE-wtCSA$^{Flag\text{-}HA}$ (+) or CS3BE-cassette1 (−) cell lysates. (**C**) Immunoblot analysis with antibodies specific for FECH or HA of immunoprecipitation (IP) samples performed with antibodies raised against FECH protein from whole cell lysates of CS3BE-wtCSA$^{Flag\text{-}HA}$ (+) or CS3BE-cassette1 (−) cells. (**D**) Immunoblot analysis with antibodies specific for FECH, CSA, CSB, DDB1, CUL4A and ROC1 of immunoprecipitation (IP) samples performed with control IgG or anti-FECH antibodies in whole cell lysate of primary dermal fibroblasts from the healthy donor C3PV.

Mutations in the *FECH* gene are associated with erythropoietic protoporphyria (EPP), an inherited disease of porphyrin-biosynthesis, characterized by severely painful phototoxic reactions due to the accumulation of protoporphyrin in the blood. Further investigations by TAP assay showed that wtCSA$^{Flag\text{-}HA}$ interacts with FECH as well as with its well-known partner DDB1 (Figure 2B). Accordingly, by using anti-FECH antibodies we found that wtCSA$^{Flag\text{-}HA}$ co-immunoprecipitates with the endogenous FECH whereas no interaction was observed in CS3BE-cassette1 cells (Figure 2C), as expected. Remarkably, in primary dermal fibroblasts from healthy donors, we repeatedly found that not only the endogenous CSA protein but also a barely detectable amount of CSB co-immunoprecipitates with FECH (Figure 2D). Conversely, we were unable to provide reliable evidence of interaction between FECH and components of CSA-core complex, such as DDB1, Cul4A and Roc1, suggesting additional functions of CSA outside the CSA-core complex.

FECH is always described as a mitochondrial protein whereas CSA has been shown to localize both in the nucleus and in mitochondria (10). To elucidate where CSA-FECH interaction takes place, we deeply investigated the subcellular localization of both proteins by immunoblotting distinct cellular fractions obtained by separating mitochon-

dria (Mit) from all other cellular compartments (Nuc/Cyt) (Figure 3A). The quality of the cell fractionation was attested by the distribution of the mitochondrial SDHA and the nuclear/cytoplasmic PCNA and c-Jun proteins. A small amount of FECH was unexpectedly found in the Nuc/Cyt fraction, although the majority of FECH is located within the mitochondria. Conversely, the wtCSA$^{Flag\text{-}HA}$ protein is present mainly in the Nuc/Cyt fraction with a weaker but clearly detectable signal in mitochondria. By immunofluorescence, we found that FECH co-localizes with the outer membrane mitochondrial protein TOMM20 in CS3BE-wtCSA$^{Flag\text{-}HA}$ cells and in normal C3PV primary fibroblasts (Figure 3B). Nevertheless, a weaker but still detectable signal is present also in the nucleus. This localization pattern is further supported by bioinformatic analysis of FECH protein sequence. cNLS Mapper indicates the presence of a monopartite nuclear localization signal (NLS) and five bipartite NLS with scores between 3 and 4.7 (Supplementary Figure S3A), predictive of protein localization to both nucleus and cytoplasm. Moreover, NucPred predicts that FECH spends at least some time in the nucleus (Supplementary Figure S3B). Therefore, FECH is both a mitochondrial and nuclear protein.

The physical interaction between FECH and wtCSA$^{Flag\text{-}HA}$ in the distinct cellular fractions (Mit and Nuc/Cyt) was investigated by immunoprecipitating FECH (Figure 3C). Despite the reduced levels of FECH outside mitochondria, a considerable amount of wtCSA$^{Flag\text{-}HA}$ is bound to FECH in the Nuc/Cyt fraction whereas a just detectable amount of wtCSA$^{Flag\text{-}HA}$ co-immunoprecipitates with FECH in mitochondria. By using anti-HA and anti-FECH antibodies, we applied the *in situ* proximity ligation assay (PLA) to visualize the CSA-FECH interaction in fixed cells. As shown by the red fluorescent dots, the two proteins interact also inside the nucleus and, apparently, in proximity of the nucleoli (Figure 3D).

UV irradiation induces a transient FECH signal at the nucleoli that requires functional CSA

Taking into account the well-established roles of CSA in UV-induced DNA damage repair and oxidative stress response, we investigated the effect of different types of stress on the FECH-wtCSA$^{Flag\text{-}HA}$ interaction by TAP experiments. In whole cell extracts, the levels of both proteins do not change following the various treatments (Supplementary Figure S4). However, the amount of FECH bound to wtCSA$^{Flag\text{-}HA}$ notably increases upon UV irradiation (10 J/m^2) but not after oxidative stress induced by either menadione (MD), a form of vitamin K that generates reactive oxygen species (ROS), or potassium bromate ($KBrO_3$), which mainly induces 8-OH-Gua (Figure 4A). Conversely, none of the genotoxic treatments influences the level of wtCSA$^{Flag\text{-}HA}$ binding to DDB1. Thus, FECH-wtCSA$^{Flag\text{-}HA}$ interaction seems to be stabilized in response to UV irradiation. A time course analysis demonstrates that the FECH-wtCSA$^{Flag\text{-}HA}$ interaction gradually increases (up to about two-fold) within the first 2 h of post-UV recovery and then rapidly returns to its basal levels (Figure 4B).

In situ PLA experiments on fixed cells reveal that the nuclear red fluorescent signal for FECH-wtCSA$^{Flag\text{-}HA}$ interaction increases in number and size at 2 h post-UV recovery, while it remains at background level in UV irradiated CS3BE-cassette1 cells (Figure 4C–D). These findings are indicative of a dynamic CSA-FECH nuclear interaction in response to UV-irradiation that prompted us to investigate whether FECH contributes to the removal of UV-induced DNA damage *via* NER. To this purpose, we took advantage of commercially available primary fibroblasts from a patient (GM05008) affected by EPP and whose deficiency of FECH activity is due to a missense mutation predicted to generate the Phe417Ser change (63) and resulting in reduced amount of FECH protein (Supplementary Figure S5A). The response of EPP cells to UV irradiation is compared to that of normal or CS primary fibroblasts by evaluating the cell post-UV survival and the efficiency of GG-NER and TC-NER by unscheduled DNA synthesis (UDS) and recovery of RNA synthesis (RRS), respectively (Supplementary Figure S5B–D). As expected, CS-A and CS-B fibroblasts show normal UDS but impaired RRS and survival levels. Conversely, the UDS, RRS and survival levels of EPP cells fall in the normal range, indicating a proper cellular response to UV irradiation. Similar results are obtained in normal fibroblasts after *FECH* expression knock-down by RNA interference. To this purpose, cells were treated with *FECH* or control (CTR) short interfering RNA (siRNA) molecules for 120 h, a time point at which FECH levels are minimal (Supplementary Figure S5E). Upon UV irradiation, fibroblasts treated with *FECH* or CTR siRNA show similar RRS values, demonstrating that impaired or reduced FECH activity does not affect the cellular response to UV exposure, including TC-NER (Supplementary Figure S5F). Therefore, the presence of CSA-FECH interaction in the nucleus must concern a role outside TC-NER.

Immunofluorescence studies were then applied to investigate the nuclear localization of FECH, its response to UV irradiation and the relationship with CSA (Figure 5). Notably, upon UV exposure a strong FECH positive signal is observed in the nucleoli of normal fibroblasts but not, or less extensively, of CS-A cells (Figure 5A-B). Time-course analysis up to 8 h post-UV recovery in four normal fibroblast strains showed that the percentage of cells with nucleolar FECH signal (nucleolar FECH$^+$ cells) drastically increases within the first 2 h after UV irradiation, with mean values ranging from 18% in unirradiated samples to about 43% in irradiated samples (Figure 5C). The number of nucleolar FECH$^+$ cells decreases to the basal level at 4 h after UV and thereafter remains constant. A different pattern is observed in fibroblasts from four CS-A donors carrying different truncating mutations. Already in basal condition the number of cells with detectable nucleolar FECH signal is lower than that of normal cultures and it gradually increases up to only 20% at 2 h after UV irradiation. A second wave of increase of nucleolar FECH$^+$ cells is observed at 4 h after UV (up to 24%), followed by a gradual decline (15%). Therefore, a functional CSA is critical for the transient UV-induced appearance of FECH inside the nucleoli. Because this event occurs in the time frame in which TC-NER takes place, we investigated the relationship between

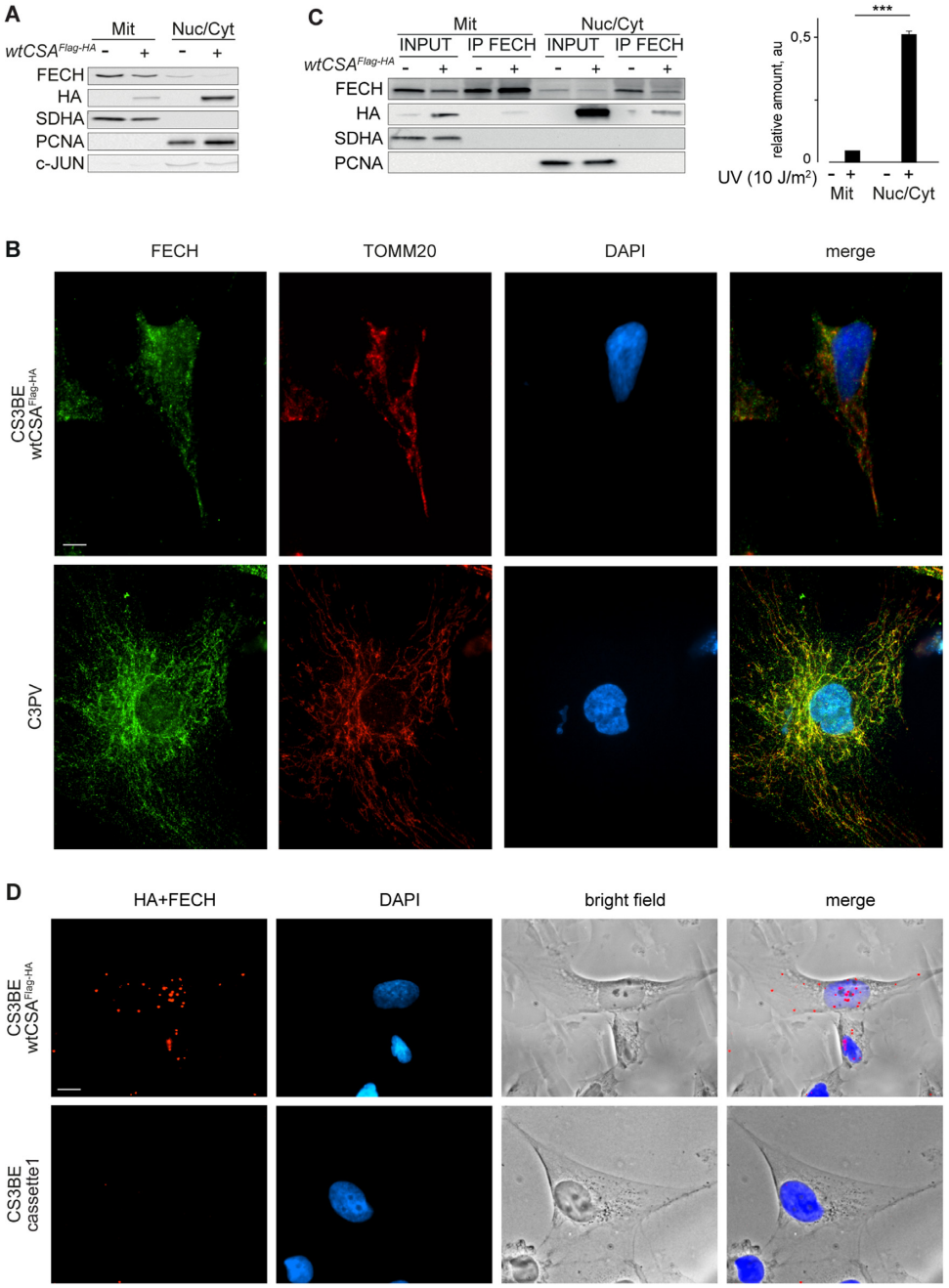

Figure 3. CSA interaction with FECH occurs mainly in the nucleus. (**A**) Immunoblot analysis of the mitochondrial fraction (Mit) separated from the remaining portion of cell lysate (Nuc/Cyt) in CS3BE-cassette1 (−) or CS3BE-wtCSA$^{Flag\text{-}HA}$ cells (+) with antibodies raised against FECH, HA, the inner membrane mitochondrial marker SDHA and the nuclear/cytosolic markers PCNA or c-JUN. (**B**) Co-immunofluorescence analysis with antibodies raised against FECH and the mitochondrial protein TOMM20 in CS3BE-wtCSA$^{Flag\text{-}HA}$ cells or in primary dermal fibroblasts from the healthy donor C3PV. Nuclei were counterstained with DAPI. Scale bar: 5 μm. (**C**) Immunoblot analysis with antibodies specific for FECH, HA, the mitochondrial marker SDHA or the nuclear/cytosolic marker PCNA in immunoprecipitations (IP) performed with anti-FECH antibodies in the mitochondrial (Mit) and nuclear/cytosolic (Nuc/Cyt) fractions (input) of CS3BE-wtCSA$^{Flag\text{-}HA}$ (+) or CS3BE-cassette1 (−) cells. The intensity of co-immunoprecipitated wtCSA$^{Flag\text{-}HA}$ band was quantified and normalized to the amount of immunoprecipitated FECH. Value are reported in the diagram on the right. Reported values represent the mean ± SEM ($n = 3$), ***$P < 0.001$ (Student's t-test). (**D**) Subcellular localization of wtCSA$^{Flag\text{-}HA}$/FECH interaction by proximity ligation assay (PLA) in CS3BE-wtCSA$^{Flag\text{-}HA}$ and CS3BE-cassette1 cells by using anti-HA and anti-FECH antibodies. Red fluorescence signal visualizes the wtCSA$^{Flag\text{-}HA}$/FECH interaction. Nuclei were counterstained with DAPI and cells visualized in bright field. Scale bar: 5 μm.

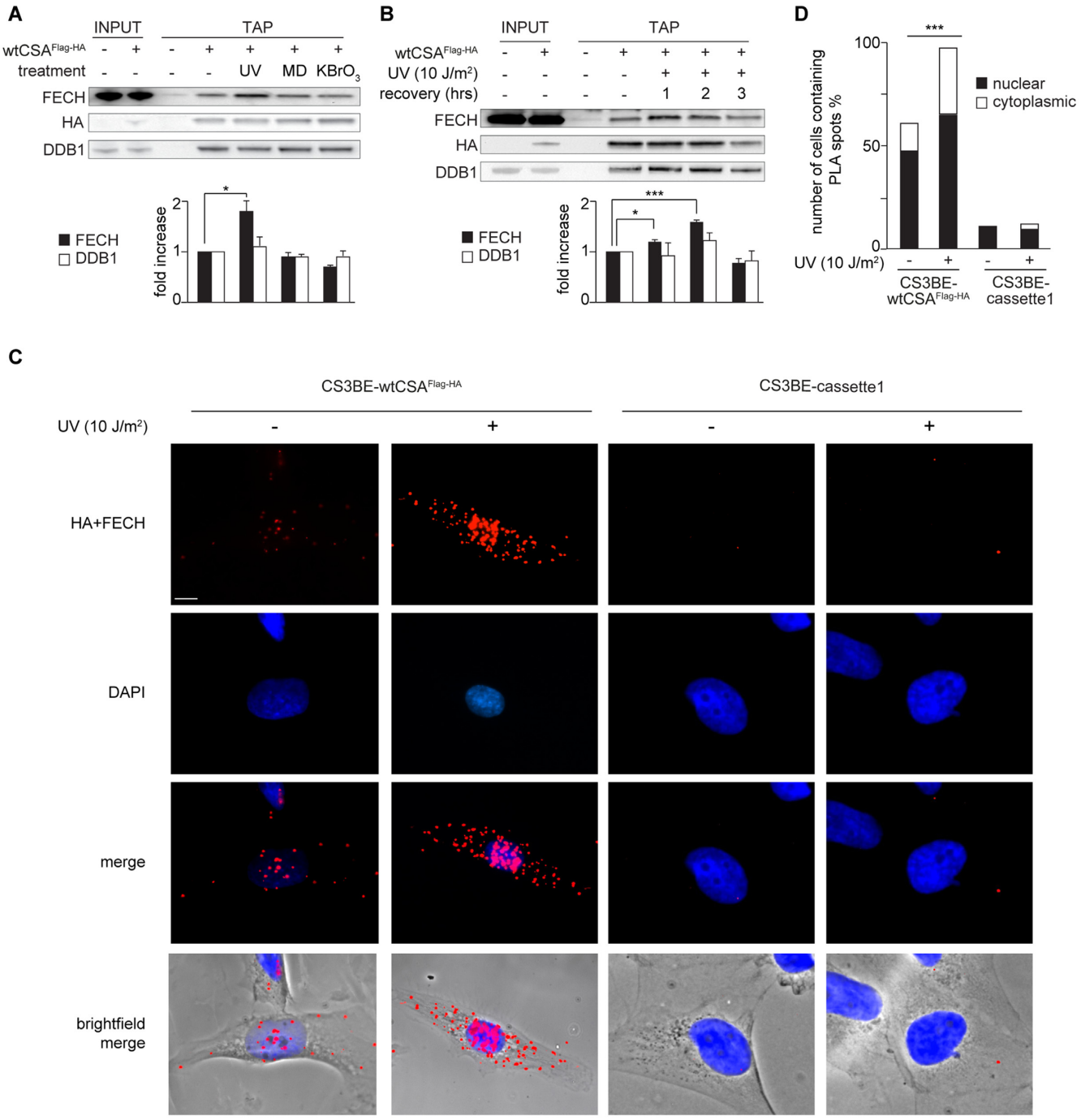

Figure 4. CSA interaction with FECH is stabilized upon UV exposure. (**A**, **B**) Immunoblot analysis with antibodies specific for FECH, HA or DDB1 of CSA$^{Flag\text{-}HA}$-interacting proteins isolated by TAP experiments in CS3BE-cassette1 (−) or CS3BE-wtCSA$^{Flag\text{-}HA}$ (+) cells before and after treatment with different stressing agents. Cells were irradiated with UV-C light (10 J/m^2) or treated with menadione (MD, 100 μM) or potassium bromate ($KBrO_3$, 20 mM) and analysed after 1 hr of recovery time (A) or at the indicated hours following UV irradiation (B). The protein levels were quantified and normalized to the corresponding HA amount and expressed as fold increase of the corresponding untreated cells. Proteins fold increase relative to the not treated sample are reported in the diagram below the plots. Reported values represent the mean ± SEM ($n = 3$), $*P < 0.05$, $***P < 0.001$ (Student's t-test). (**C**) Sub-cellular localization of wtCSA$^{Flag\text{-}HA}$/FECH interaction by proximity ligation assay (PLA) with anti-HA and anti-FECH antibodies in CS3BE-wtCSA$^{Flag\text{-}HA}$ and CS3BE-cassette1 cells before and at 2 h of UV irradiation (10 J/m^2). Red fluorescence signal visualizes the CSA/FECH interaction. Nuclei were counterstained with DAPI and cells visualized in bright field. Scale bar: 5 μm. (**D**) Number of cells containing the PLA spots shown in C and expressed as percentage. In each sample 100 cells have been analyzed. The percentage of nuclear and cytoplasmic spots is indicated.

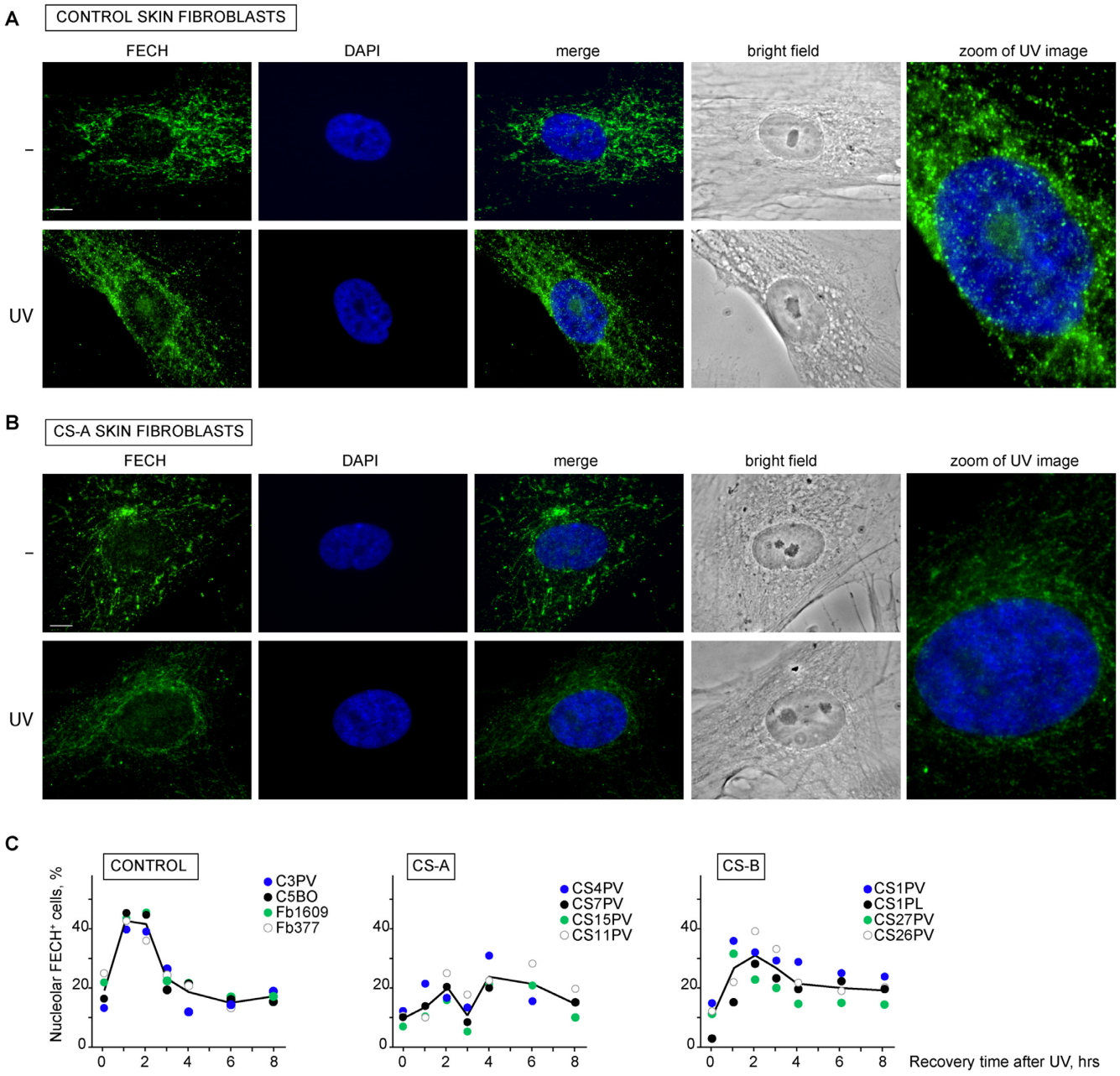

Figure 5. CSA functionality allows FECH visibility in the nucleolus upon UV irradiation. (**A, B**) Immunofluorescence analysis with antibodies specific for FECH protein in primary dermal fibroblasts from the healthy donor C3PV (A) or the CSA-defective CS15PV patient (**B**), cultured under basal conditions or at 2 h after UV-C irradiation (10 J/m^2). Nuclei were counterstained with DAPI and cells visualized in bright field. (**C**) Percentage of cells showing FECH accumulation in nucleoli (nucleolar FECH$^+$ cells) of primary dermal fibroblasts from C3PV, C5BO, Fb1609 and Fb377 healthy donors (Normal), CS4PV, CS7PV, CS15PV, CS11PV patients (CS-A) and CS1PV, CS1PL, CS27PV, CS26PV patients (CS-B) before and at different time points (1, 2, 3, 4, 6 and 8 h) after UV irradiation (10 J/m^2). For each strain at least 200 nuclei were counted and the mean value of at least two independent experiments is shown at each point. The black line represents the mean value of all strains and all experiments. SE is below 10% in all cases. Scale bar: 5 μm.

FECH positive signal at the nucleolus and functional TC-NER by analysing four CS-B fibroblast strains that are also TC-NER defective but express a functional CSA protein. In CS-B cultures, the percentage of nucleolar FECH$^+$ cells approaches the levels detected in normal fibroblasts, with a rapid increase in the mean value up to the 31% at 2 h after UV irradiation. Overall, these findings indicate that in UV-irradiated human fibroblasts the transient appearance of FECH at the nucleoli requires CSA. This transient signal may reflect either a UV-induced recruitment of the protein itself within the nucleoli or changes in the pattern of FECH-interacting proteins leading to epitope unmasking. The separation of nucleolar extract from the nucleoplasm, mitochondria and remaining cellular components, demonstrates the presence of FECH inside nucleoli of normal skin fibroblasts already in basal condition and denies any incre-

ment of the protein at 2 h after UV irradiation (Supplementary Figure S6). Besides demonstrating that FECH is also a nucleolar protein, these findings indicate that CSA may impact on the protein-protein interaction network of FECH inside the nucleoli.

CSA$^{Flag\text{-}HA}$ and FECH form a protein complex with RNAP1, CSB, RPS15 and RPS10, a fraction of which dissociates from the chromatin after UV irradiation

In the mass spectrometry analysis of CSA-interacting proteins we found four ribosomal proteins of the small 40S ribosome subunits (RPS10, RPS15, RPS28 and RPSA, see Supplementary Table S8), which are known to enter the nucleolus in order to assemble with the ribosomal RNA (rRNA). The ability of CSA to bind ribosomal proteins has also been recently reported (35). Thus, we investigated whether FECH also interacts with the other nucleolar CSA-binding proteins. By co-immunoprecipitation experiments we found that RPS10 and RPS15 proteins interact with FECH in the nuclear compartment but not in the cytoplasm (Figure 6A). No interaction is observed between FECH and RPS28 or RPSA, suggesting the formation of a nucleolar protein complex involving CSA, FECH and specific ribosomal proteins (RPs). Knowing that CSA, similarly to CSB, is a transcription factor of RNAP1 (18,31), we investigated whether nuclear FECH also interacts with RNAP1 and/or CSB. Indeed, both the catalytic subunit of RNAP1 (RPA194) and CSB co-immunoprecipitate with FECH in the nuclear compartment (Figure 6A), indicating that CSA–FECH–RNAP1–CSB–RPS15–RPS10 may belong to a unique protein complex. Similarly, RNAP1 co-immunoprecipitates FECH in total nuclear extracts (Supplementary Figure S7). Since rRNA synthesis and ribosomal biogenesis take place on the chromatin template, we investigated the complex composition associated to the chromatin. Thus, native chromatin was separated from the TritonX100-soluble fraction of CS3BE-cassette1 and CS3BE-wtCSA$^{Flag\text{-}HA}$ cells lysed with the Triton Lysis Buffer. The same procedure was applied to CS1AN cells that are compound heterozygous for mutations in the *ERCC6/CSB* gene leading to the altered forms p.Lys337* and p.Tyr834Cysfs*25 of CSB. In all cell lines we found considerable amounts of FECH, RNAP1, RPS10 and RPS15 associated to the chromatin marked by the presence of the histone H3 (Figure 6B). CSA$^{Flag\text{-}HA}$ protein is bound to the chromatin of CS3BE-wtCSA$^{Flag\text{-}HA}$ cells; wild type CSB to the chromatin of CS3BE-cassette1 and CS3BE-wtCSA$^{Flag\text{-}HA}$ cells (Supplementary Figure S8A) while the mutated p.Tyr834Cysfs*25 form of CSB is found associated to the chromatin-enriched fraction of CS1AN cells (Figure 6B). As expected, the cytosolic MEK2 and mitochondrial SDHA markers are predominantly found in the soluble fractions. At 2 h after UV irradiation the amount of the chromatin-associated FECH, CSA$^{Flag\text{-}HA}$, RNAP1, CSB, RPS10 and RPS15 is significantly reduced in CSA expressing cells (CS3BE-wtCSA$^{Flag\text{-}HA}$ and CS1AN) while most of them preserve their interaction with the chromatin in CSA-defective cells (CS3BE-cassette1). This indicates that after UV irradiation a functional CSA is required to trigger the detachment from the chromatin of a fraction of the aforementioned proteins.

To understand whether FECH, CSA$^{Flag\text{-}HA}$, RNAP1, CSB, RPS10 and RPS15 are part of a unique chromatin-bound protein complex, we performed a series of co-immunoprecipitations from native chromatin before and after exposing the cells to UV irradiation. Co-immunoprecipitated proteins have been normalized to the amount of immunoprecipitated FECH (Figure 7A and Supplementary S8B-C), immunoprecipitated RNAP1 (Figure 7B) or immunoprecipitated CSB (Supplementary Figure S8D). While no interactions are found in the soluble fractions, a significantly larger amount of RNAP1, RPS10 and RPS15 interact with the chromatin-bound FECH as well as with the chromatin-bound CSB in CS3BE-wtCSA$^{Flag\text{-}HA}$ compared to CS3BE-cassette1 cells (Figure 7A and Supplementary Figure S8B, D). Thus, CSA favours the formation of this large chromatin-associated protein complex. Differently from FECH and CSB, the amount of chromatin-bound RNAP1 interactors is similar (for RPS15) or even higher (for FECH, CSB and RPS10) in CS3BE-cassette1 compared to CS3BE-wtCSA$^{Flag\text{-}HA}$ cells (Figure 7B), indicating once more that the lack of CSA impairs the composition of the RNAP1-containing complex.

At 2 h after UV irradiation the binding of FECH to RNAP1, CSB, RPS10 and RPS15 on the chromatin of CSA-expressing cells is reduced while no significant reductions are observed in the absence of CSA (Figure 7A and Supplementary Figure S8B, C). Similar results were achieved by immunoprecipitating the chromatin-bound RNAP1 or CSB (Figure 7B and S8D), further supporting our previous observation that the presence of CSA favours the dissociation of a fraction of the complex from the chromatin after UV exposure (Figure 6B). Meanwhile, FECH slightly increases its binding to the chromatin-bound wtCSA$^{Flag\text{-}HA}$ (Figure 7A and Supplementary Figure S8B, C).

Finally, a two-step co-immunoprecipitation (TIP) experiment performed by first immunoprecipitating FECH and subsequently RNAP1 from the native chromatin of control primary dermal fibroblasts fully demonstrates that FECH–RNAP1–CSA–CSB–RPS15–RPS10 are all part of a unique chromatin-bound protein complex (Figure 7C). The direct interaction between FECH and RNAP1, the influence of CSA and the partial dissociation of FECH-RNAP1 binding at 2 h after UV irradiation have also been observed by PLA analysis in CS3BE-cassette1 and CS3BE-wtCSA$^{Flag\text{-}HA}$ cells (Figure 7D and Supplementary Figure S9).

In summary, these findings demonstrate that in normal cells there is a protein complex on the nucleolar chromatin that includes FECH, RNAP1, CSA, CSB, RPS10 and RPS15. Upon UV irradiation a fraction of this protein complex dissociates from the chromatin and disaggregates. The chromatin-bound FECH partially loses its interaction with RNAP1 but retains its binding to wtCSA$^{Flag\text{-}HA}$. The absence of CSA affects the composition of this RNAP1-contining complex and impairs its release from the chromatin upon UV irradiation.

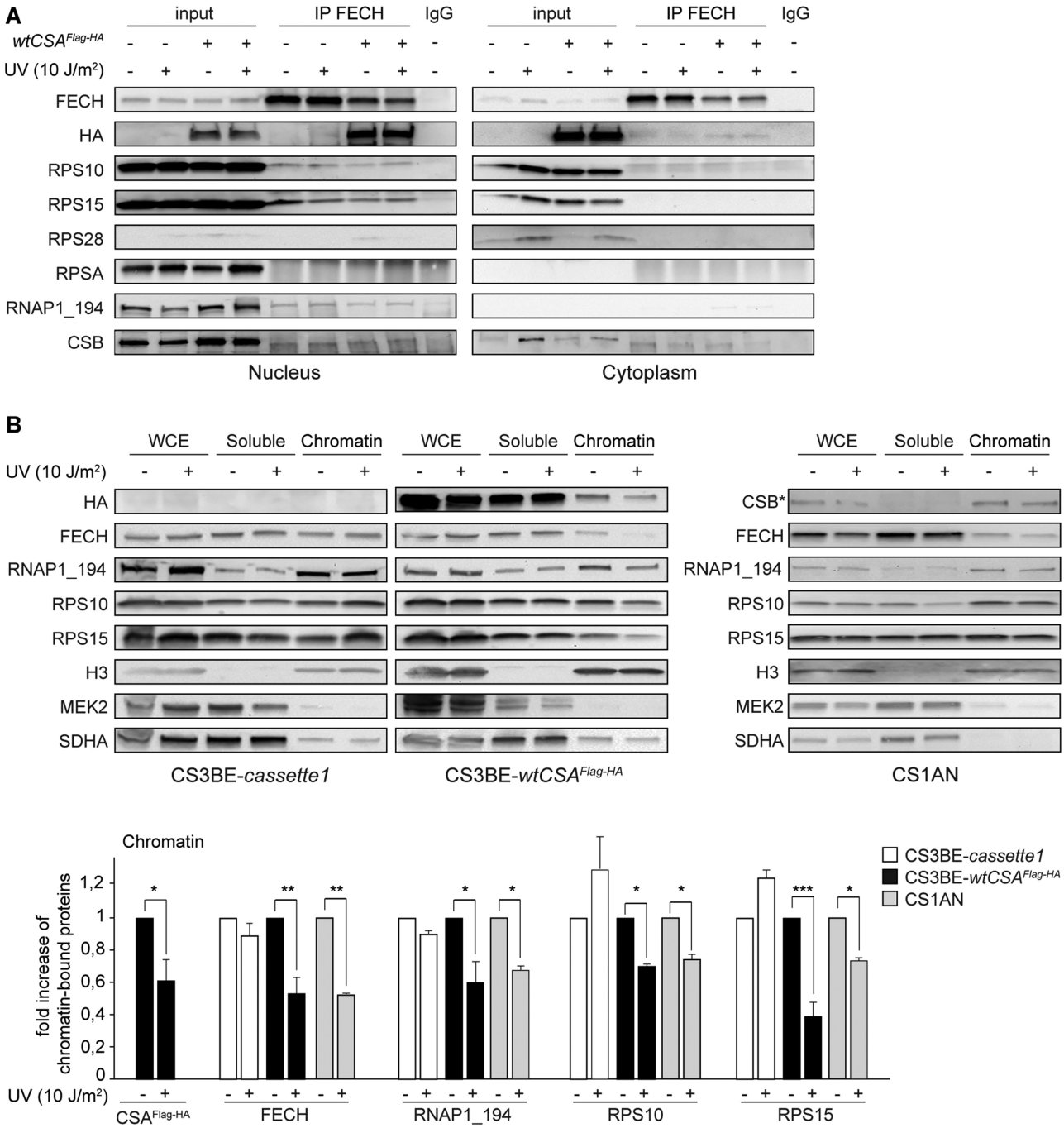

Figure 6. FECH and CSA bind to RNAP1 and specific ribonuclear proteins. (**A**) Immunoblot analysis with antibodies specific for FECH, HA, the ribosomal proteins RPSl0, RPS15, RPS28, RPSA, the catalytic subunit of RNAP1 (RNAP1) and CSB in immunoprecipitations (IP) performed with anti-FECH antibodies in the nuclear and cytoplasmatic fractions (input) of CS3BE-wtCSA$^{Flag\text{-}HA}$ (+) or CS3BE-cassette1 (−) cells, before (−) and 2 h after 10 J/m^2 UV irradiation (+). (**B**) Immunoblot analysis of the whole cell extract (WCE), the 1% TritonX100-soluble (Soluble) and insoluble (Chromatin-enriched) fractions of CS3BE-wtCSA$^{Flag\text{-}HA}$, CS3BE-cassette1 and CS1AN cell lines, before (−) and 2 h after 10 J/m^2 UV irradiation (+) with antibodies raised against FECH, the catalytic subunit of RNAP1 (RNAP1_194), RPS10, RPS15, the chromatin bound protein histone 3 (H3), the cytosolic protein MEK2 and the inner membrane mitochondrial marker SDHA. In CS1AN cells the CSB antibody recognizes the mutated p.Tyr834Cysfs*25 form of the protein (CSB*). The levels of proteins in the chromatin-enriched fractions was quantified and normalized to the level of the corresponding chromatin-bound H3 and expressed in the diagram on the right as fold increase of the corresponding untreated cells. Reported values represent the mean ± SEM ($n = 3$), *$P < 0.05$, **$P < 0.01$, ***$P < 0.001$ (Student's t-test).

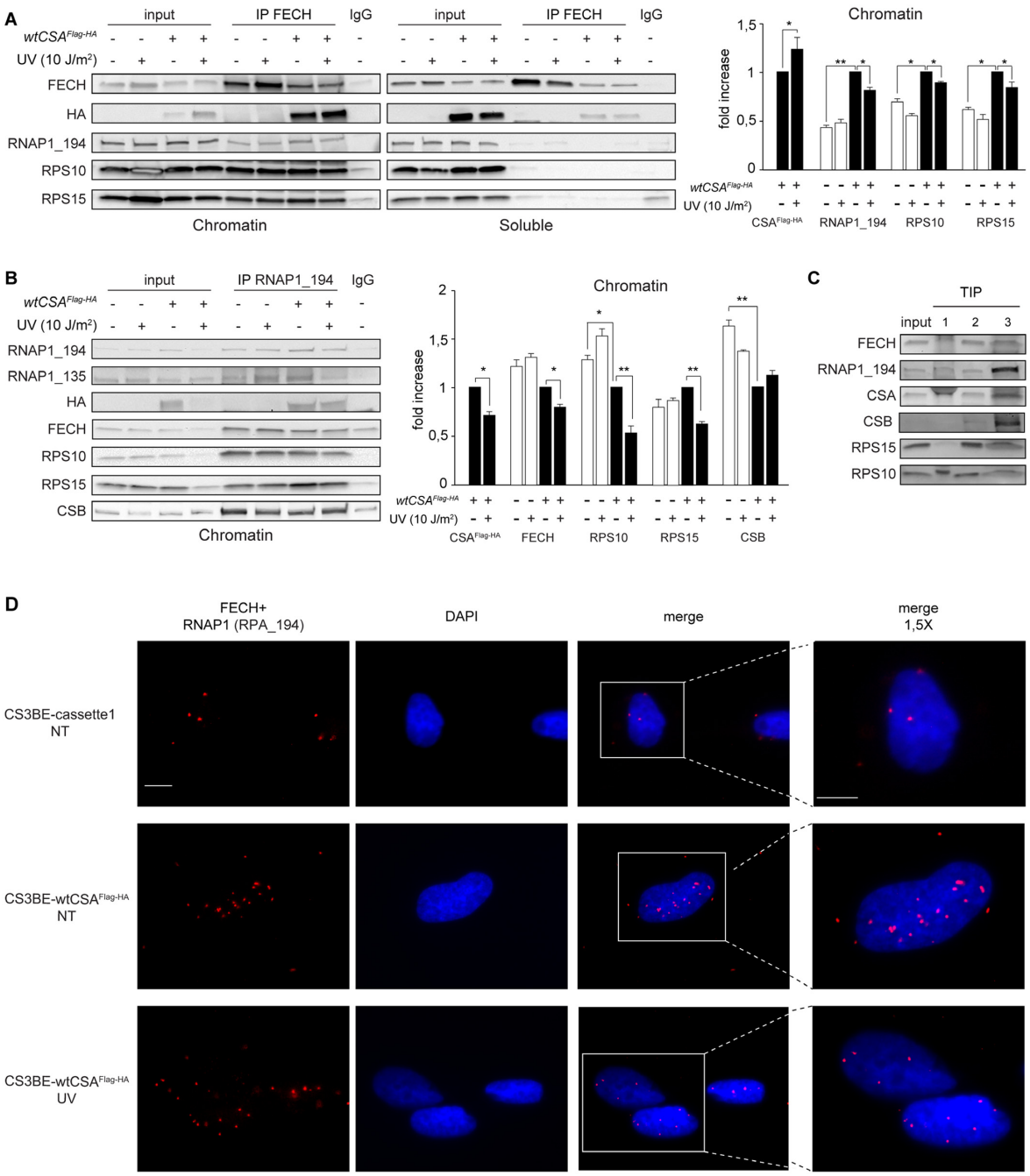

Figure 7. CSA favours the formation of the FECH-CSA-CSB-RNAP1-RPS protein complex on native chromatin and its dissociation upon UV irradiation. (**A**) Immunoblot analysis with antibodies specific for FECH, HA, the catalytic subunit of RNAP1 (RNAP1_194), RPS10 and RPS15 in immunoprecipitations (IP) performed with anti-FECH antibodies or control IgG in the chromatin-enriched or TritonX100-soluble fractions (input) of CS3BE-wtCSA$^{Flag\text{-}HA}$ (+) or CS3BE-cassette1 (−) cells, before (−) and after 10 J/m^2 UV irradiation (+). The amount of co-immunoprecipitated proteins was quantified and normalized to the amount of immunoprecipitated FECH and expressed in the diagram on the right as fold increase of the corresponding co-immunoprecipitated protein in CS3BE-wtCSA$^{Flag\text{-}HA}$ untreated cells. Reported values represent the mean ± SEM ($n = 4$), *$P < 0.05$, **$P < 0.01$ (Student's t-test). (**B**) Immunoblot analysis with antibodies specific for the catalytic and the RPA135 subunits of RNAP1 (RNAP1_194 and RNAP1_135, respectively), HA, FECH, RPS10, RPS15 and CSB in immunoprecipitations (IP) performed with anti-RNAP1_194 antibodies or control IgG in the chromatin-enriched fractions (input) of CS3BE-wtCSA$^{Flag\text{-}HA}$ (+) or CS3BE-cassette1 (−) cells, before (−) and after 10 J/m^2 UV irradiation (+). The amount of co-immunoprecipitated proteins was quantified and normalized to the amount of immunoprecipitated RNAP1 and expressed in the diagram on the right as fold increase of the corresponding co-immunoprecipitated protein in CS3BE-wtCSA$^{Flag\text{-}HA}$ untreated cells. Reported values represent the mean ± SEM ($n = 4$), *$P < 0.05$, **$P < 0.01$ (Student's t-test). (**C**) Immunoblot analysis with antibodies specific for FECH, the catalytic subunit of RNAP1 (RNAP1_194), CSA, CSB, RPS15 and RPS10 in two-step co-immunoprecipitations (TIP) performed first by immunoprecipitating with anti-RNAP1_194 (2) antibodies and subsequently with anti-FECH (3) antibodies in the chromatin-enriched fractions (input) of primary dermal fibroblasts from an healthy donor. The immunoprecipitation with IgG (1) antibodies is a negative control. (**D**) Sub-cellular localization of FECH/RNAP1 interaction by proximity ligation assay (PLA) in CS3BE-wtCSA$^{Flag\text{-}HA}$ (+) and CS3BE-cassette1 (−) cells, before (−) and at 2 h after UV irradiation (10 J/m^2). Red fluorescence signal visualizes the FECH/RNAP1 interaction. Nuclei were counterstained with DAPI. Scale bar: 10 μm.

FECH is a regulator of ribosomal transcription

The influence of CSA and FECH proteins on RNAP1 activity has been investigated by chromatin immunoprecipitation (ChIP), *in situ* run-on experiments, northern blot and real time RT-PCR. A reduced recruitment of RNAP1 on two distinct regions of the rDNA repeat, the first mapping at the 5′ of the transcribed region (47S) and the second one on the 5.8S coding sequence, is found by ChIP assays in CS3BE-cassette1 compared to CS3BE-wtCSA$^{Flag\text{-}HA}$ cells (Figure 8A). As expected, no RNAP1 recruitment is observed in the intragenic (IGS) rDNA regions. The reduced occupancy of RNAP1 on the rDNA repeat of CS3BE-cassette1 strongly supports the knowledge that CSA impairment affects RNAP1 activity (31). Differently from our previous finding showing that a fraction of RNAP1-containing complex dissociates from the entire chromatin of CS3BE-wtCSA$^{Flag\text{-}HA}$ at 2 h after UV exposure (Figures 6B and 7B), no significant changes of RNAP1 occupancy are observed on 47S and 5.8S amplicons after UV. Likely, the amount of few RNAP1 complexes detaching from a single amplicon as a consequence of UV-induced DNA lesions is below the level of detection by ChIP assay. Notably, either *CSA* or *FECH* silencing in CS3BE-wtCSA$^{Flag\text{-}HA}$ cells results in reduced binding of RNAP1 to the rDNA, thus demonstrating that nucleolar FECH is important for proper RNAP1 activity (Figure 8B).

Next, pre-rRNA synthesis has been evaluated by *in situ* run-on experiments in primary fibroblasts from healthy individuals (Normal), CS-A or EPP patients. Fibroblasts were treated with the adenosine analogue DRB (5,6-dichloro-1-beta-D-ribofuranosylbenzimidazole) to abolish the RNAP2-dependent transcription. As previously demonstrated (31), all CS-A cells display reduced pre-rRNA transcription, corresponding to about 50% of normal (Figure 8C and Supplementary Figure S10). Remarkably, EPP primary fibroblasts display an intense nucleolar signal, almost four times stronger than that of normal fibroblasts, indicative of drastically increased levels of pre-rRNA in these cells. This observation was further corroborated by showing that in normal C3PV fibroblasts the amount of ribosomal transcripts increases four times upon *FECH* silencing whereas it is unaffected following CTR siRNA treatment (Figure 8D and Supplementary Figure S10). Notably, silencing the endogenous *CSA* gene in EPP cells is sufficient to reduce the high levels of basal ribosomal transcription, indicating the essential and upstream role of CSA in RNAP1 transcription.

Since the reduced occupancy of RNAP1 on rDNA contradicts the paralleled increased amount of pre-rRNA in *FECH* silenced cells, we hypothesize that FECH may play a role in regulating pre-rRNA processing and ribosome maturation. Thus, we performed northern blot analysis on total RNA extracted from CS3BE-wtCSA$^{Flag\text{-}HA}$ cells after gene expression silencing with control (CTR) siRNA or with *FECH*, *CSA*, *RPS10* or *RPS15* siRNA (Figure 8E). Compared to CTR siRNA treatment, all the other samples revealed a significantly reduced amount of 47S, consistent with the reduced RNAP1 occupancy on rDNA (Figure 8A, B). However, the normalization of the 18S pre-rRNA precursors (30S, 21S and 18S-E) to the amount of the corresponding 47S revealed a tendency of *FECH, RPS10* and *RPS15* silenced cells to accumulate the 18S-E pre-rRNA (Figure 8E), an event that is indicative of an altered pre-rRNAs processing. To further corroborate this finding, we investigated the amount of 18S transcripts in primary dermal fibroblasts from CSA-defective or FECH-defective patients by real time RT-PCR analysis. The total RNA-derived cDNA samples were amplified with primers specific for the 5′ transcript (47S), the 18S rRNA and the housekeeper genes *GAPDH*. Compared to control fibroblasts, a strong reduction of 47S pre-rRNA is found in both CS-A and EPP cells that in *FECH*-mutated cells is however associated to a strong accumulation of 18S rRNA (Figure 8F). The diverse content of 18S rRNA in CS-A and EPP cells may easily explain the different rRNA levels previously detected by *in situ* run-on experiments (Figure 8C, D). Overall, the present data demonstrate the concerted action of FECH and CSA proteins in tightly regulating RNAP1 activity and ribosome biogenesis.

DISCUSSION

In the present study, we generated isogenic cell lines diverging only for the expression of *CSA*$^{Flag\text{-}HA}$, which were instrumental for the identification of FECH as novel interactor of CSA and its striking role in the nucleolar compartment. The CSA-FECH interaction does not involve DDB1 or other components of the CSA-core complex but RNAP1, CSB, RPS10 and RPS15. As a member of the WD40-repeat protein family, CSA folds into a β-propeller structure that provides a platform for the assembly of protein complexes or acts as mediator of transient interplay among other proteins (7,64–68). Here, we show that CSA interacts with partners not implicated in TC-NER and participate to a large chromatin-bound protein complex whose function is to regulate rRNA synthesis and ribosome biogenesis. After protein synthesis, most ribosomal proteins (RPs) are transported from the cytoplasm to the nucleus where, in a coordinated manner and together with copious transcription factors, associate to rRNA precursors (pre-rRNA) giving rise to the multistep process that leads to the formation of ribonucleoparticles. While CSA binds at least four RPs (namely RPS10, RPS15, RPS28 and RPSA) of the small 40S subunit, FECH binds only RPS10 and RPS15, suggesting that not all the proteins of the complex directly interact with FECH or, alternatively, that the participation of FECH to the CSA–CSB–RNAP1–RPs complex might occur in a shorter period of time compared to CSA. RPS28 is undetectable in the nuclear fraction (Figure 6A) thus explaining the lack of interaction with the chromatin bound FECH.

The functional CSA favours the interaction of FECH as well as CSB to RNAP1–RPS10–RPS15 on the chromatin (Figure 7 and Supplementary Figure S8), an event that parallels the more efficient RNAP1 ribosomal transcription in CSA expressing cells (Figure 8) and in line with the idea that CSA is relevant for an efficient RNAP1 activity (18–20,24,31). Similarly to *CSA*, *FECH* silencing leads to reduced RNAP1 occupancy on rDNA and reduced 47S pre-rRNA synthesis but, compared to CSA, FECH impairment results in a strong increment of 18S-E pre-rRNAs (Figure 8

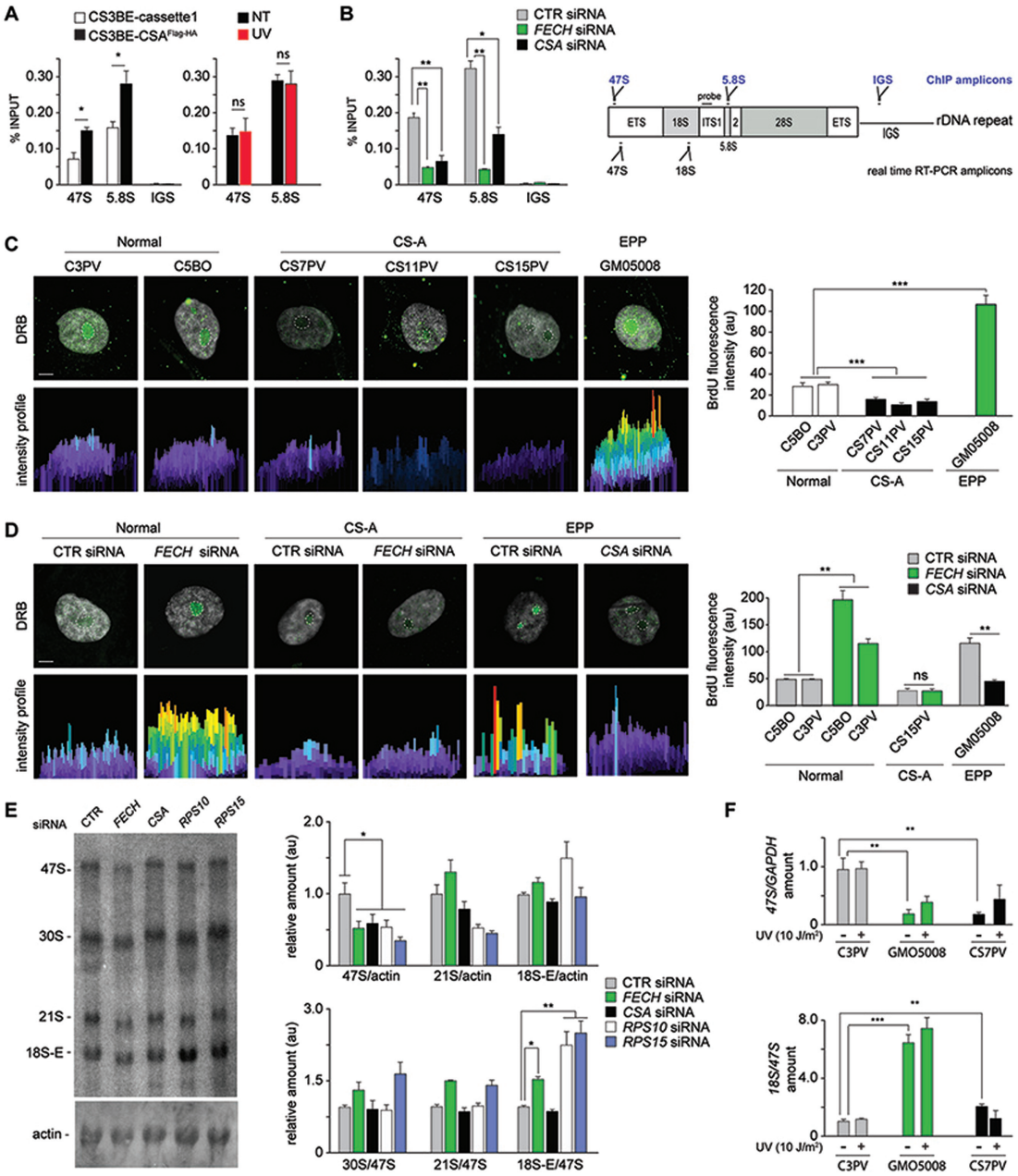

Figure 8. FECH is a regulator of ribosomal transcription. (**A, B**) RNAP1 occupancy on 47S, 5.8S and intergenic spacer (IGS) of the rDNA repeat in CS3BE-cassette1 and CS3BE-wtCSA$^{Flag\text{-}HA}$ cells (A, *left panel*), in CS3BE-wtCSA$^{Flag\text{-}HA}$ under basal condition and at 2 h after UV irradiation (A, *right panel*) and in CS3BE-wtCSA$^{Flag\text{-}HA}$ cells after treatment for 120 h with control (CTR), *FECH* or *CSA* siRNA molecules (B). The occupancy identified by ChIP analysis is expressed as percentage of the input after subtraction of the corresponding background value (IgG antibody). Reported values represent the mean ± SEM ($n = 3$), $*P < 0.05$, $**P < 0.01$, ns = not statistically significant (Student's t-test). On the right of panel B, a schematic representation of the rDNA repeat indicating the position of the ChIP amplicons (*bleu*), the probe for the northern blot described in (E) and the real time RT-PCR amplicons (*black*) described in (F); (**C, D**) Representative images of nucleolar run-on transcription assay in Dichlororibo-furanosyl (DRB)-treated primary fibroblast from normal (C3PV or C5BO), CS-A (CS7PV, CS11PV or CS15PV) or erythropoietic protoporphyria (EPP, GMO5008) cells before (C) or after treatment for 120 h with control (CTR), *FECH* or *CSA* siRNA molecules (D). The incorporation of bromodeoxyuridine (BrdU) was visualized by indirect immunofluorescence with anti-BrdU antibodies. Images were obtained by overlaying the DAPI stained nucleus (gray) with the corresponding BrdU fluorescence (green). The nucleolar fluorescence intensity was visualized as intensity profile with the MetaMorph software, measured with the ImageJ software and represented in the diagram on the right (au: arbitrary units). Reported values represent the mean ± SEM ($n = 20$), $**P < 0.01$, $***P < 0.001$, ns: not significant (Student's t-test). Scale bar: 5μm. (**E**) Northern blot analysis of CS3BE-wtCSA$^{Flag\text{-}HA}$ treated for 72 h with control (CTR), *FECH*, *CSA*, *RPS10* or *RPS15* siRNA and hybridized with the ITS1 probe indicated in (A). The intensity of rRNA precursor bands has been quantified and normalized to the intensity of the corresponding actin band or to the 47S band and reported on the diagrams on the right. Reported values represent the mean ± SEM ($n = 3$), $*P < 0.05$, $**P < 0.01$ (Student's *t*-test). (**F**) Real time RT-PCR analysis of 47S and 18S rRNA levels in primary dermal fibroblasts from an healthy individual (C3PV), an EPP (GMO5008) and CS-A patient (CS7PV) before (−) and after 10 J/m^2 UV irradiation (+). The 47S transcript levels were normalized to the expression level of the corresponding housekeeping gene *GAPDH* (*top*) while the 18S transcript levels were normalized to the expression level of the corresponding 47S (*middle* and *bottom*, respectively). Reported values represent the mean ± SEM ($n = 4$), $**P < 0.01$, $***P < 0.001$ (Student's *t*-test).

and Supplementary Figure S10), indicating a role for FECH in pre-rRNA processing. These differences may explain the apparently opposite nucleolar transcription efficiency in CS and EPP cells by *in situ* run-on experiments (Figure 8C-D). Notably, *CSA* knock down reduces the pre-RNA accumulation in EPP cells (Figure 8D), strengthening the upstream role of CSA in rRNA synthesis. A reduced 47S transcription and an accumulation of 18S-E rRNA is also observed upon *RPS10* or *RPS15* silencing, in agreement with previous findings (69).

FECH has always been reported as a mitochondrial protein that localizes both in the inner and outer membranes (70). Here we show that FECH also localizes inside the nucleus (Figures 3A, 4C, 5, 6 and 7), as predicted by bioinformatics analysis (Supplementary Figure S3). The human ferrochelatase is a homodimer that catalyses the insertion of Fe^{2+} into protoporphyrin IX (71). Its interaction with the iron-loaded frataxin is essential for the cellular regulation of iron homeostasis and heme biosynthesis (72). Although Fe^{2+} is the physiological substrate of FECH, the enzyme can also bind and catalyse the insertion of other divalent metal ions into the porphyrin macrocycle, including Zn^{2+}, Ni^{2+}, Cu^{2+} and Co^{2+} (72,73). Since under physiological conditions many enzymes rely on the presence of divalent metal ions to fulfil their activities, it is tempting to speculate that FECH may influence the enzymatic activity of neighbouring proteins by locally sequestering or *vice versa* by specifically loading metal ions on target proteins. Notably, the single amino acid substitution F417S responsible for EPP (GM05008 patient (63)) impairs both the heme biosynthesis as well as the rRNA processing (Figure 8).

After exposing cells to UV irradiation, we observe a reduction of the CSA–FECH–CSB–RNAP1–RPS10–RPS15 complex associated to the chromatin of $wtCSA^{Flag\text{-}HA}$ expressing cells (Figures 6B, 7A, B and S8). The chromatin fractionation has been performed under native conditions in order to avoid unspecific protein-DNA crosslinking. The presence of UV-induced DNA lesions can interfere with the progression of RNAP1 transcription (74,75) causing an arrest or a dislocation of RNAP1 from the chromatin in order to provide the time and space for the removal of photoproducts from the rDNA (76). While much is known about TC-NER operating on the transcribed strand of active genes by RNAP2, the events implicated in RNAP1 transcription arrest and UV-induced rDNA damage processing are still elusive. In general, DNA damage, including photolesions, is processed less efficiently in rRNA genes than in RNAP2 transcribed genes and total genome (77,78). Here, we show that upon UV irradiation a fraction of RNAP1 dissociates from the chromatin in a CSA-dependent manner (Figure 6B) indicating that CSA not only is a transcription factor for RNAP1 but also plays a role in the first events that follow the stalling of RNAP1 in front rDNA photolesions. Even if stably associated to CSA, FECH is not implicated in the NER pathway (Supplementary Figure S5). By immunofluorescence we observe an accumulation of FECH inside the nucleoli at 2 h after UV exposure (Figure 5). However, such accumulation is not detected by immunoblotting in fractionated nucleoli (Supplementary Figure S6). This discrepancy indicates that the intensified immunofluorescence signal does not derive from increased amounts of FECH inside the nucleoli but more likely from changes in its pattern of interactions that result in a less masked FECH, now available for antibody recognition. Indeed, we found that upon UV irradiation FECH maintains its binding to CSA but partially dissociates from RNAP1, CSB and RPS proteins (Figure 7 and Supplementary Figure S8). In CSA-defective cells the FECH–RNAP1–CSB–RPS10–RPS15 complex maintains its association to the chromatin even after UV exposure thus explaining the lack of $FECH^{+}$ nucleoli (Figure 5). Overall, our findings disclose an unexpected role of FECH inside the nucleoli where it acts in cooperation with CSA, CSB, RNAP1, RPS10 and RPS15 to regulate rRNA synthesis and processing. With its dual localization, FECH belongs to the network of proteins that create a link between mitochondrial metabolic activities and gene expression regulation (79).

SUPPLEMENTARY DATA

Supplementary Data are available at NAR Online.

FUNDING

Associazione Italiana per la Ricerca sul Cancro (AIRC) [IG 21737 to D.O. and 13537 to M.S.]; Superpig project Fund for Promoting Institutional Agreements/Regione Lombardia and PRIN [2008P772PW_002 to F.P]; Fondazione Buzzati Traverso for one-year fellowship to M.L. Funding for open access charge: Associazione Italiana per la Ricerca sul Cancro [21737].
Conflict of interest statement. None declared.

REFERENCES

1. Laugel,V. (2013) Cockayne syndrome: the expanding clinical and mutational spectrum. *Mech. Ageing Dev.*, **134**, 161–170.
2. Karikkineth,A.C., Scheibye-Knudsen,M., Fivenson,E., Croteau,D.L. and Bohr,V.A. (2017) Cockayne syndrome: clinical features, model systems and pathways. *Ageing Res. Rev.*, **33**, 3–17.
3. Calmels,N., Botta,E., Jia,N., Fawcett,H., Nardo,T., Nakazawa,Y., Lanzafame,M., Moriwaki,S., Sugita,K., Kubota,M. *et al.* (2018) Functional and clinical relevance of novel mutations in a large cohort of patients with Cockayne syndrome. *J. Med. Genet.*, **55**, 329–343.
4. Marteijn,J.A., Lans,H., Vermeulen,W. and Hoeijmakers,J.H.J. (2014) Understanding nucleotide excision repair and its roles in cancer and ageing. *Nat. Rev. Mol. Cell Biol.*, **15**, 465–481.
5. Lake,R.J. and Fan,H.-Y. (2013) Structure, function and regulation of CSB: a multi-talented gymnast. *Mech. Ageing Dev.*, **134**, 202–211.
6. Groisman,R., Kuraoka,I., Chevallier,O., Gaye,N., Magnaldo,T., Tanaka,K., Kisselev,A.F., Harel-Bellan,A. and Nakatani,Y. (2006) CSA-dependent degradation of CSB by the ubiquitin-proteasome pathway establishes a link between complementation factors of the Cockayne syndrome. *Genes Dev.*, **20**, 1429–1434.
7. Fischer,E.S., Scrima,A., Böhm,K., Matsumoto,S., Lingaraju,G.M., Faty,M., Yasuda,T., Cavadini,S., Wakasugi,M., Hanaoka,F. *et al.* (2011) The molecular basis of CRL4DDB2/CSA ubiquitin ligase architecture, targeting, and activation. *Cell*, **147**, 1024–1039.
8. Epanchintsev,A., Costanzo,F., Rauschendorf,M.-A., Caputo,M., Ye,T., Donnio,L.-M., Proietti De Santis,L., Coin,F., Laugel,V. and Egly,J.M. (2017) Cockayne's syndrome A and B proteins regulate transcription arrest after genotoxic stress by promoting ATF3 degradation. *Mol. Cell*, **68**, 1054–1066.e6.
9. Lanzafame,M., Vaz,B., Nardo,T., Botta,E., orioli,D. and Stefanini,M. (2013) From laboratory tests to functional characterisation of Cockayne syndrome. *Mech. Ageing Dev.*, **134**, 171–179.

10. Kamenisch,Y., Fousteri,M., Knoch,J., von Thaler,A.-K., Fehrenbacher,B., Kato,H., Becker,T., Dollé,M.E.T., Kuiper,R., Majora,M. *et al.* (2010) Proteins of nucleotide and base excision repair pathways interact in mitochondria to protect from loss of subcutaneous fat, a hallmark of aging. *J. Exp. Med.*, **207**, 379–390.
11. Aamann,M.D., Sorensen,M.M., Hvitby,C., Berquist,B.R., Muftuoglu,M., Tian,J., de Souza-Pinto,N.C., Scheibye-Knudsen,M., Wilson,D.M., Stevnsner,T. *et al.* (2010) Cockayne syndrome group B protein promotes mitochondrial DNA stability by supporting the DNA repair association with the mitochondrial membrane. *FASEB J.*, **24**, 2334–2346.
12. Menoni,H., Wienholz,F., Theil,A.F., Janssens,R.C., Lans,H., Campalans,A., Radicella,J.P., Marteijn,J.A. and Vermeulen,W. (2018) The transcription-coupled DNA repair-initiating protein CSB promotes XRCC1 recruitment to oxidative DNA damage. *Nucleic. Acids. Res.*, **46**, 7747–7756.
13. Boetefuer,E.L., Lake,R.J. and Fan,H.-Y. (2018) Mechanistic insights into the regulation of transcription and transcription-coupled DNA repair by Cockayne syndrome protein B. *Nucleic Acids Res.*, **46**, 7471–7479.
14. Crochemore,C., Fernández-Molina,C., Montagne,B., Salles,A. and Ricchetti,M. (2019) CSB promoter downregulation via histone H3 hypoacetylation is an early determinant of replicative senescence. *Nat. Commun.*, **10**, 5576–5517.
15. Balajee,A.S., May,A., Dianov,G.L., Friedberg,E.C. and Bohr,V.A. (1997) Reduced RNA polymerase II transcription in intact and permeabilized Cockayne syndrome group B cells. *Proc. Natl. Acad. Sci. U.S.A.*, **94**, 4306–4311.
16. van Gool,A.J., Citterio,E., Rademakers,S., van Os,R., Vermeulen,W., Constantinou,A., Egly,J.M., Bootsma,D. and Hoeijmakers,J.H. (1997) The Cockayne syndrome B protein, involved in transcription-coupled DNA repair, resides in an RNA polymerase II-containing complex. *EMBO J.*, **16**, 5955–5965.
17. Selby,C.P. and Sancar,A. (1997) Cockayne syndrome group B protein enhances elongation by RNA polymerase II. *Proc. Natl. Acad. Sci. U.S.A.*, **94**, 11205–11209.
18. Bradsher,J., Auriol,J., Proietti De Santis,L., Iben,S., Vonesch,J.L., Grummt,I. and Egly,J.M. (2002) CSB is a component of RNA pol I transcription. *Mol. Cell*, **10**, 819–829.
19. Yuan,X., Feng,W., Imhof,A., Grummt,I. and Zhou,Y. (2007) Activation of RNA polymerase I transcription by cockayne syndrome group B protein and histone methyltransferase G9a. *Mol. Cell*, **27**, 585–595.
20. Lebedev,A., Scharffetter-Kochanek,K. and Iben,S. (2008) Truncated Cockayne syndrome B protein represses elongation by RNA polymerase I. *J. Mol. Biol.*, **382**, 266–274.
21. Berquist,B.R., Canugovi,C., Sykora,P., Wilson,D.M. and Bohr,V.A. (2012) Human Cockayne syndrome B protein reciprocally communicates with mitochondrial proteins and promotes transcriptional elongation. *Nucleic Acids Res.*, **40**, 8392–8405.
22. Vélez-Cruz,R. and Egly,J.M. (2013) Cockayne syndrome group B (CSB) protein: at the crossroads of transcriptional networks. *Mech. Ageing Dev.*, **134**, 234–242.
23. Cho,I., Tsai,P.-F., Lake,R.J., Basheer,A. and Fan,H.-Y. (2013) ATP-dependent chromatin remodeling by Cockayne syndrome protein B and NAP1-like histone chaperones is required for efficient transcription-coupled DNA repair. *PLos Genet.*, **9**, e1003407.
24. Scheibye-Knudsen,M., Tseng,A., Borch Jensen,M., Scheibye-Alsing,K., Fang,E.F., Iyama,T., Bharti,S.K., Marosi,K., Froetscher,L., Kassahun,H. *et al.* (2016) Cockayne syndrome group A and B proteins converge on transcription-linked resolution of non-B DNA. *Proc. Natl. Acad. Sci. U.S.A.*, **113**, 12502–12507.
25. D'Errico,M., Parlanti,E., Teson,M., Degan,P., Lemma,T., Calcagnile,A., Iavarone,I., Jaruga,P., Ropolo,M., Pedrini,A.M. *et al.* (2007) The role of CSA in the response to oxidative DNA damage in human cells. *Oncogene*, **26**, 4336–4343.
26. Scheibye-Knudsen,M., Ramamoorthy,M., Sykora,P., Maynard,S., Lin,P.-C., Minor,R.K., Wilson,D.M., Cooper,M., Spencer,R., de Cabo,R. *et al.* (2012) Cockayne syndrome group B protein prevents the accumulation of damaged mitochondria by promoting mitochondrial autophagy. *J. Exp. Med.*, **209**, 855–869.
27. D'Errico,M., Pascucci,B., Iorio,E., Van Houten,B. and Dogliotti,E. (2013) The role of CSA and CSB protein in the oxidative stress response. *Mech. Ageing Dev.*, **134**, 261–269.
28. Khobta,A. and Epe,B. (2013) Repair of oxidatively generated DNA damage in Cockayne syndrome. *Mech. Ageing Dev.*, **134**, 253–260.
29. Cleaver,J.E., Brennan-Minnella,A.M., Swanson,R.A., Fong,K.-W., Chen,J., Chou,K.-M., Chen,Y.-W., Revet,I. and Bezrookove,V. (2014) Mitochondrial reactive oxygen species are scavenged by Cockayne syndrome B protein in human fibroblasts without nuclear DNA damage. *Proc. Natl. Acad. Sci. U.S.A.*, **111**, 13487–13492.
30. Chatre,L., Biard,D.S.F., Sarasin,A. and Ricchetti,M. (2015) Reversal of mitochondrial defects with CSB-dependent serine protease inhibitors in patient cells of the progeroid Cockayne syndrome. *Proc. Natl. Acad. Sci. U.S.A.*, **112**, E2910–E2919.
31. Koch,S., Garcia Gonzalez,O., Assfalg,R., Schelling,A., Schäfer,P., Scharffetter-Kochanek,K. and Iben,S. (2014) Cockayne syndrome protein A is a transcription factor of RNA polymerase I and stimulates ribosomal biogenesis and growth. *Cell Cycle*, **13**, 2029–2037.
32. Okur,M.N., Lee,J.-H., Osmani,W., Kimura,R., Demarest,T.G., Croteau,D.L. and Bohr,V.A. (2020) Cockayne syndrome group A and B proteins function in rRNA transcription through nucleolin regulation. *Nucleic Acids Res.*, **48**, 2473–2485.
33. Alupei,M.C., Maity,P., Esser,P.R., Krikki,I., Tuorto,F., Parlato,R., Penzo,M., Schelling,A., Laugel,V., Montanaro,L. *et al.* (2018) Loss of proteostasis is a pathomechanism in cockayne syndrome. *Cell Rep.*, **23**, 1612–1619.
34. Phan,T., Khalid,F. and Iben,S. (2019) Nucleolar and ribosomal dysfunction - a common pathomechanism in childhood progerias? *Cells*, **8**, 534.
35. Qiang,M., Khalid,F., Phan,T., Ludwig,C., Scharffetter-Kochanek,K. and Iben,S. (2021) Cockayne syndrome-associated CSA and CSB mutations impair ribosome biogenesis, ribosomal protein stability, and global protein folding. *Cells*, **10**, 1616.
36. Holme,S.A., Anstey,A.V., Finlay,A.Y., Elder,G.H. and Badminton,M.N. (2006) Erythropoietic protoporphyria in the U.K.: clinical features and effect on quality of life. *Br. J. Dermatol.*, **155**, 574–581.
37. Casanova-González,M.J., Trapero-Marugán,M., Jones,E.A. and Moreno-Otero,R. (2010) Liver disease and erythropoietic protoporphyria: a concise review. *World J. Gastroenterol.*, **16**, 4526–4531.
38. Lane,A.M., McKay,J.T. and Bonkovsky,H.L. (2016) Advances in the management of erythropoietic protoporphyria - role of afamelanotide. *Appl Clin Genet*, **9**, 179–189.
39. Adam,M.P., Ardinger,H.H., Pagon,R.A., Wallace,S.E., Bean,L.J., Mefford,H.C., Stephens,K., Amemiya,A., Ledbetter,N., Balwani,M. *et al.* (1993) *Erythropoietic Protoporphyria, Autosomal Recessive*.
40. Pasquier,L., Laugel,V., Lazaro,L., Dollfus,H., Journel,H., Edery,P., Goldenberg,A., Martin,D., Heron,D., Le Merrer,M. *et al.* (2006) Wide clinical variability among 13 new Cockayne syndrome cases confirmed by biochemical assays. *Arch. Dis. Child.*, **91**, 178–182.
41. Sarasin,A., Blanchet-Bardon,C., Renault,G., Lehmann,A., Arlett,C. and Dumez,Y. (1992) Prenatal diagnosis in a subset of trichothiodystrophy patients defective in DNA repair. *Br. J. Dermatol.*, **127**, 485–491.
42. Stefanini,M., Giliani,S., Nardo,T., Marinoni,S., Nazzaro,V., Rizzo,R. and Trevisan,G. (1992) DNA repair investigations in nine Italian patients affected by trichothiodystrophy. *Mutat. Res.*, **273**, 119–125.
43. Stefanini,M., Fawcett,H., Botta,E., Nardo,T. and Lehmann,A.R. (1996) Genetic analysis of twenty-two patients with Cockayne syndrome. *Hum. Genet.*, **97**, 418–423.
44. Colbere-Garapin,F., Chousterman,S., Horodniceanu,F., Kourilsky,P. and Garapin,A.C. (1979) Cloning of the active thymidine kinase gene of herpes simplex virus type 1 in Escherichia coli K-12. *Proc. Natl. Acad. Sci. U.S.A.*, **76**, 3755–3759.
45. Paixão,S., Colaluca,I.N., Cubells,M., Peverali,F.A., Destro,A., Giadrossi,S., Giacca,M., Falaschi,A., Riva,S. and Biamonti,G. (2004) Modular structure of the human lamin B2 replicator. *Mol. Cell. Biol.*, **24**, 2958–2967.
46. Lauth,M., Spreafico,F., Dethleffsen,K. and Meyer,M. (2002) Stable and efficient cassette exchange under non-selectable conditions by combined use of two site-specific recombinases. *Nucleic. Acids. Res.*, **30**, e115.
47. Lanzafame,M., Botta,E., Teson,M., Fortugno,P., Zambruno,G., Stefanini,M. and orioli,D. (2015) Reference genes for gene expression

analysis in proliferating and differentiating human keratinocytes. *Exp. Dermatol.*, **24**, 314–316.
48. Potter,C.J. and Luo,L. (2010) Splinkerette PCR for mapping transposable elements in Drosophila. *PLoS One*, **5**, e10168.
49. Schneider,C.A., Rasband,W.S. and Eliceiri,K.W. (2012) NIH Image to ImageJ: 25 years of image analysis. *Nat. Methods*, **9**, 671–675.
50. Wansink,D.G., Schul,W., van der Kraan,I., van Steensel,B., van Driel,R. and de Jong,L. (1993) Fluorescent labeling of nascent RNA reveals transcription by RNA polymerase II in domains scattered throughout the nucleus. *J. Cell Biol.*, **122**, 283–293.
51. Rosner,M., Schipany,K. and Hengstschläger,M. (2013) Merging high-quality biochemical fractionation with a refined flow cytometry approach to monitor nucleocytoplasmic protein expression throughout the unperturbed mammalian cell cycle. *Nat. Protoc.*, **8**, 602–626.
52. ten Have,S., Hodge,K. and Lamond,A.I. (2012) In: Meroni,G. and Petrera,F. (eds). *Dynamic Proteomics: Methodologies and Analysis*, IntechOpen.
53. Orioli,D., Colaluca,I.N., Stefanini,M., Riva,S., Dotti,C.G. and Peverali,F.A. (2006) Rac3-induced neuritogenesis requires binding to Neurabin I. *Mol. Biol. Cell*, **17**, 2391–2400.
54. Arseni,L., Lanzafame,M., Compe,E., Fortugno,P., Afonso-Barroso,A., Peverali,F.A., Lehmann,A.R., Zambruno,G., Egly,J.M., Stefanini,M. *et al.* (2015) TFIIH-dependent MMP-1 overexpression in trichothiodystrophy leads to extracellular matrix alterations in patient skin. *Proc. Natl. Acad. Sci. U.S.A.*, **112**, 1499–1504.
55. Orioli,D., Compe,E., Nardo,T., Mura,M., Giraudon,C., Botta,E., Arrigoni,L., Peverali,F.A., Egly,J.M. and Stefanini,M. (2013) XPD mutations in trichothiodystrophy hamper collagen VI expression and reveal a role of TFIIH in transcription derepression. *Hum. Mol. Genet.*, **22**, 1061–1073.
56. Landi,C., Bargagli,E., Carleo,A., Bianchi,L., Gagliardi,A., Cillis,G., Perari,M.G., Refini,R.M., Prasse,A., Bini,L. *et al.* (2015) A functional proteomics approach to the comprehension of sarcoidosis. *J. Proteomics*, **128**, 375–387.
57. Sinha,P., Poland,J., Schnölzer,M. and Rabilloud,T. (2001) A new silver staining apparatus and procedure for matrix-assisted laser desorption/ionization-time of flight analysis of proteins after two-dimensional electrophoresis. *Proteomics*, **1**, 835–840.
58. Peverali,F.A., Orioli,D., Tonon,L., Ciana,P., Bunone,G., Negri,M. and Della-Valle,G. (1996) Retinoic acid-induced growth arrest and differentiation of neuroblastoma cells are counteracted by N-myc and enhanced by max overexpressions. *Oncogene*, **12**, 457–462.
59. Kosugi,S., Hasebe,M., Tomita,M. and Yanagawa,H. (2009) Systematic identification of cell cycle-dependent yeast nucleocytoplasmic shuttling proteins by prediction of composite motifs. *Proc. Natl. Acad. Sci. U.S.A.*, **106**, 10171–10176.
60. Brameier,M., Krings,A. and MacCallum,R.M. (2007) NucPred–predicting nuclear localization of proteins. *Bioinformatics*, **23**, 1159–1160.
61. Ajioka,R.S., Phillips,J.D. and Kushner,J.P. (2006) Biosynthesis of heme in mammals. *Biochim. Biophys. Acta*, **1763**, 723–736.
62. Hamza,I. and Dailey,H.A. (2012) One ring to rule them all: trafficking of heme and heme synthesis intermediates in the metazoans. *Biochim. Biophys. Acta*, **1823**, 1617–1632.
63. Brenner,D.A., Didier,J.M., Frasier,F., Christensen,S.R., Evans,G.A. and Dailey,H.A. (1992) A molecular defect in human protoporphyria. *Am. J. Hum. Genet.*, **50**, 1203–1210.
64. Henning,K.A., Li,L., Iyer,N., McDaniel,L.D., Reagan,M.S., Legerski,R., Schultz,R.A., Stefanini,M., Lehmann,A.R., Mayne,L.V. *et al.* (1995) The Cockayne syndrome group A gene encodes a WD repeat protein that interacts with CSB protein and a subunit of RNA polymerase II TFIIH. *Cell*, **82**, 555–564.
65. Li,D. and Roberts,R. (2001) WD-repeat proteins: structure characteristics, biological function, and their involvement in human diseases. *Cell. Mol. Life Sci.*, **58**, 2085–2097.
66. Smith,T.F. (2008) Diversity of WD-repeat proteins. *Subcell. Biochem.*, **48**, 20–30.
67. Xu,C. and Min,J. (2011) Structure and function of WD40 domain proteins. *Protein Cell*, **2**, 202–214.
68. Wang,Y., Hu,X.-J., Zou,X.-D., Wu,X.-H., Ye,Z.-Q. and Wu,Y.-D. (2015) WDSPdb: a database for WD40-repeat proteins. *Nucleic. Acids. Res.*, **43**, D339–D344.
69. O'Donohue,M.-F., Choesmel,V., Faubladier,M., Fichant,G. and Gleizes,P.-E. (2010) Functional dichotomy of ribosomal proteins during the synthesis of mammalian 40S ribosomal subunits. *J. Cell Biol.*, **190**, 853–866.
70. Sakaino,M., Ishigaki,M., Ohgari,Y., Kitajima,S., Masaki,R., Yamamoto,A. and Taketani,S. (2009) Dual mitochondrial localization and different roles of the reversible reaction of mammalian ferrochelatase. *FEBS J.*, **276**, 5559–5570.
71. Burden,A.E., Wu,C., Dailey,T.A., Busch,J.L., Dhawan,I.K., Rose,J.P., Wang,B. and Dailey,H.A. (1999) Human ferrochelatase: crystallization, characterization of the [2Fe-2S] cluster and determination that the enzyme is a homodimer. *Biochim. Biophys. Acta*, **1435**, 191–197.
72. Söderberg,C., Gillam,M.E., Ahlgren,E.-C., Hunter,G.A., Gakh,O., Isaya,G., Ferreira,G.C. and Al-Karadaghi,S. (2016) The structure of the complex between yeast frataxin and ferrochelatase: characterization and pre-steady state reaction of ferrous iron delivery and heme synthesis. *J. Biol. Chem.*, **291**, 11887–11898.
73. Al-Karadaghi,S., Franco,R., Hansson,M., Shelnutt,J.A., Isaya,G. and Ferreira,G.C. (2006) Chelatases: distort to select? *Trends Biochem. Sci.*, **31**, 135–142.
74. Conconi,A., Bespalov,V.A. and Smerdon,M.J. (2002) Transcription-coupled repair in RNA polymerase I-transcribed genes of yeast. *Proc. Natl. Acad. Sci. U.S.A.*, **99**, 649–654.
75. Hanawalt,P.C. and Spivak,G. (2008) Transcription-coupled DNA repair: two decades of progress and surprises. *Nat. Rev. Mol. Cell Biol.*, **9**, 958–970.
76. Daniel,L., Cerrutti,E., Donnio,L.-M., Nonnekens,J., Carrat,C., Zahova,S., Mari,P.-O. and Giglia-Mari,G. (2018) Mechanistic insights in transcription-coupled nucleotide excision repair of ribosomal DNA. *Proc. Natl Acad. Sci. U.S.A.*, **115**, E7650.
77. Charton,R., Guintini,L., Peyresaubes,F. and Conconi,A. (2015) Repair of UV induced DNA lesions in ribosomal gene chromatin and the role of 'Odd' RNA polymerases (I and III). *DNA Repair (Amst.)*, **36**, 49–58.
78. Tsekrekou,M., Stratigi,K. and Chatzinikolaou,G. (2017) The nucleolus: in genome maintenance and repair. *Int. J. Mol. Sci.*, **18**, 1411.
79. Monaghan,R.M. and Whitmarsh,A.J. (2015) Mitochondrial proteins moonlighting in the nucleus. *Trends Biochem. Sci.*, **40**, 728–735.